Am J Transl Res 2023;15(4):2345-2369
www.ajtr.org /ISSN:1943-8141/AJTR0147364

*Original Article*

# Multicellular network analysis of melanoma heterogeneity by scRNA-seq

Shun Li[1,2], Long Chen[1,2]

[1]*Department of Immunology, School of Basic Medical Sciences, Chengdu Medical College, Chengdu 610500, Sichuan, China;* [2]*Non-Coding RNA and Drug Discovery Key Laboratory of Sichuan Province, Chengdu Medical College, Chengdu 610500, Sichuan, China*

Received October 30, 2022; Accepted January 30, 2023; Epub April 15, 2023; Published April 30, 2023

**Abstract:** Objective: Melanoma neoplasia is a complicated process. Not only melanocytes are involved, stromal cells and immune cells would also regulate cancer development. However, the cell type composition and tumor immune microenvironment of melanoma are poorly understood. Method: Here we report a map of the cellular landscape of human melanoma via analyzing published single-cell RNA sequencing (scRNA-seq) dataset. Transcriptional profiles of 4645 cells obtained from 19 melanoma tissues were dissected. Result: Using gene expression patterns and flow cytometry, 8 discrete cell populations were identified including endothelial cells (ECs), cancer related fibroblasts (CAFs), macrophages, B cells, T cells (NK cells), memory T cells (MTCs), melanocytes and podocytes. By constructing the cell-specific network (CSN) for each cell population, scRNA-seq data can be used for clustering and pseudotrajectory analyzing from network perspective. In addition, the differentially expressed genes (DEGs) between malignant and non-malignant melanocytes were identified and analyzed together with clinical data from The Cancer Genome Atlas (TCGA). Conclusion: This study shows a comprehensive view of melanoma at the single cell resolution which outlines the characteristics of resident cells in tumor. Particular, it provides an immune microenvironment map of melanoma.

**Keywords:** Melanoma, network, scRNA-seq, heterogeneity, immune cell

## Introduction

Tumors are complex ecosystems defined as spatiotemporal interactions between heterogeneous cell types, including stromal cells, malignant cells and tumor-infiltrating lymphocytes (TILs) [1, 2]. Tumor cellular diversity poses both challenges and opportunities for melanoma therapy. It has been suggested that recurrences and drug tolerance-induced treatment failures may be derived from intratumor heterogeneity [3]. Different cell composition patterns in tumors, as well as interactions and substance signaling among different cell types, may play a key role in the malignant development of melanoma and the cause of drug resistance [4]. However, their significant biological function in the specific cellular components and the pathway by which they collectively define the behavior of melanoma remains unclear.

Cancer therapy might be accelerated by technologies that assess the malignant, micro-environmental, and immunologic states most likely to be informative about cancer development, treatment response and resistance. Previously, tumor state would be assessed by quantifying variation in oncogenic signaling pathways according to the mixed dataset of immune, stromal and other cells. Compared with scRNA-seq, traditional RNA-seq and network analysis methods are limited to heterogeneous cells instead of single cells and result in the erased character of each cell population. Single-cell genomic approaches enable detailed evaluation of genetic and transcriptional features presented in individual cells per tumor. In principle, this approach may identify all major cellular components simultaneously, the heterogeneity and functional diversity among cell populations can be revealed and new cell types with distinct functions may be discovered [5-8].

Here, we analyzed the intratumoral heterogeneity in melanoma using published scRNA-seq [9]. In our study, both malignant and non-malignant

cell types and states, their drivers and interrelationships in the complex tumor cellular ecosystem were explored. In addition, differentially expressed genes (DEGs) of each cell subtype were identified and specific networks about the pathway, biological process (BP), cellular component (CC) and molecular function (MF) were also constructed. By combining with the clinical dataset in TCGA, the significance of DEGs was further confirmed. A reference map of the melanoma landscape at single-cell resolution is critical to understanding the pathogenesis and treatment. This transcriptomic map serves as a fundamental baseline description for human melanoma (**Sketch Map 1**).

## Methods

### *ScRNA-seq and data processing*

Science the experiment details were described in Tirosh's paper, we thus introduce the whole process in brief. Resected tumors were rinsed with PBS and transported in DMEM on ice immediately after surgical procurement. Small fragments were stored in RNA-protect for bulk RNA and DNA isolation. Tumor pieces were digested for 10 minutes at 37°C, then vortexed for 10 seconds and pipetted up and down for 1 min using pipettes. After filtering with 70 μm nylon mesh, the suspension was supplemented with 30 ml PBS include 2% fetal calf serum (FCS) and immediately placed on ice. After centrifuging at 580 g at 4°C for 6 minutes, the supernatant was discarded and the cell pellet was re-suspended in PBS.

After sorted single cells via FACS, RNA and DNA were isolated using Qiagen mini kit following the manufacturer's recommendations. Whole transcriptome amplification (WTA) was performed with a modified SMART-Seq2 protocol [10, 11]. WTA products were cleaned with Agencourt XP DNA beads and 70% ethanol and Illumina sequencing libraries were prepared using Nextera XT (Illumina, San Diego, CA). Whole-exome of samples were sequenced on an Illumina NextSeq 500 instrument using 30 bp paired-end reads. All sample pairs passed the Firehose pipeline including a QC pipeline to test for any tumor/normal and inter-individual contamination as previously described [14, 15]. The MuTect algorithm was used to identify somatic mutations [15] and reduce false positive cells. Somatic mutations including single-nucleotide variants, insertions, and deletions were annotated using Oncotator [16].

### *T-SNE analysis and cell type classification*

ALONA (https://alona.panglaodb.se/index.html) is a cloud-based bioinformatics service designed to analyze scRNA-seq data. ALONA performs advanced visualization, processing and cell type prediction from scRNA-seq using machine learning models to achieve accurate inference of biological cell types. ALONA currently works with scRNA-seq data from mouse and human. We upload processed files with default parameters (hard thresholds of quality filtering, median cell cluster statistic, small cluster resolution and without removing mitochondrial genes). In 2D-t-SNE map, cells were clustered and colored by cell type based on unique marker genes. After analysis, the top 20 expressed genes and marker genes per cluster were also listed.

In addition to ALONA, another online interactive software named ASAP (Automated Single-cell Analysis Pipeline, https://asap.epfl.ch/) was also used in our study. ASAP combines a wide range of commonly used algorithms with sophisticated visualization tools. It allows researchers to interact with the data in a straightforward fashion and in real time [18]. Once uploaded sequencing files with filtering and normalization, t-SNE map was generated with default parameters (perplexity = 30 and theta = 0.5). Trajectory analysis could be performed with a global gene set via DDRTree reduction method and the single cell was colored by state or pseudotime.

To identify sub-clusters within these eight cell types, we reanalyzed cells belonging to each of these types separately. Specifically, we applied dimensionality reduction in each cell type using t-SNE analysis from ALONA with default parameters. Each cell type was reclustered by its principle components. Notably, sub-clustering was robust to alterations in the number of principal components, in the resolution or in the K parameter. We next inputted group files obtain from ALONA and screened DEGs with FDR $\leq$ 0.05 and fold change $\geq$ 2.

### *Comprehensive analysis of cell type-specific functions*

To assess differential activities of pathways or gene ontology (GO) between sets of cells (for

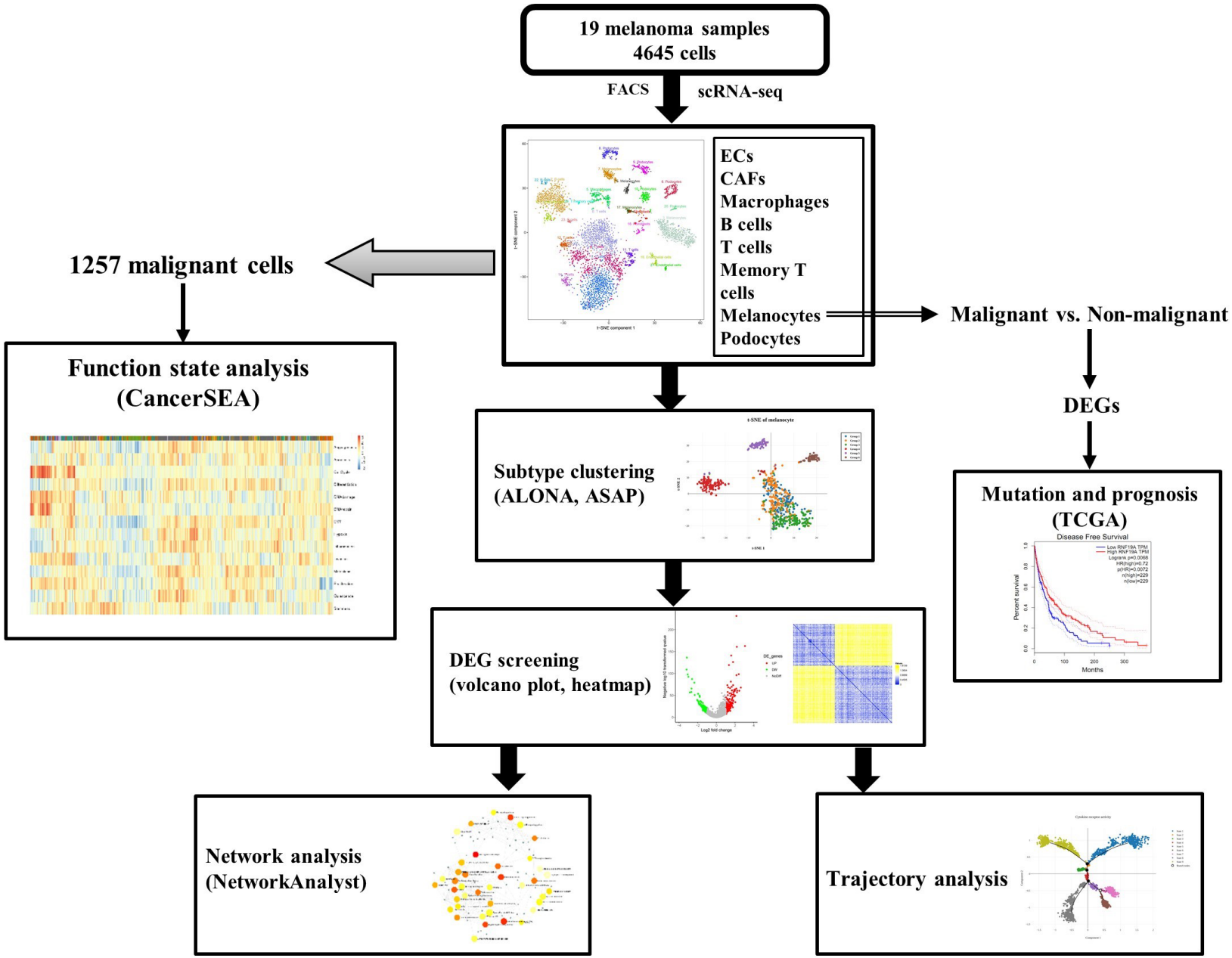


**Sketch Map 1.** The sketch map of workflow.

example, derived from malignant or non-malignant cells, or belonging to different sub-clusters), DEGs visualized with volcano plots or heatmaps should be identified firstly from ASAP. NetworkAnalyst (https://www.networkanalyst.ca/NetworkAnalyst/faces/home.xhtml) [19], a visual analytics platform for comprehensive gene expression profiling were used to enrich significant pathways and GO functions (Benjamini-Hochberg-corrected *p*-value < 0.05) which compared with DAVID results (https://david.ncifcrf.gov/). Click "Gene list input" button and input DEGs include up- and down-regulated genes followed by DEGs-pathways or -GOs networks constructed which were significantly regulated.

To assess the role of DEGs in melanoma patients, the expression of them in bulk RNA-seq data from TCGA were abtained. Briefly, in cBioPortal (https://www.cbioportal.org/), sequencing data of 479 melanoma patients were selected to test the role and variation of DEGs in different melanocyte subtype (i.e. malignant vs. non-malignant). In addition, via GEPIA (gene expression profiling interactive analysis, http://gepia.cancer-pku.cn/index.html), the survivorship curves (overall survival and disease-free survival) of DEGs were calculated with median group cutoff (50% cutoff-high, 50% cutoff-low) [20]. Furthermore, the immunohistochemical results of specific genes in melanoma were obtained from The Human Protein Atlas (https://www.proteinatlas.org/).

*Statistical analysis*

Statistical analysis for zonation figures was performed using GraphPad Prism v5.0. The utilized statistical test is listed in each figure caption. The melanoma sequencing samples from TCGA database were adequate because sufficient power using equivalent tests was observed in a previous study. To test for differential expression across two groups (tumor and normal), the R package DESeq2 was used on raw count data [21]. For comparison of 2 groups, the two-side Student's t-test and Wilcoxon-rank sum test was used. The *p*-values were adjusted by the Benjamini-Hochberg method. ***P < 0.001, **P < 0.01, *P < 0.05, ns = not significance (P > 0.05).

## Results

*The landscape of individual cells in melanoma*

Tumor mass is made up of tumor cells but also stromal cells that enable them to live and grow, endothelial cells, infiltrating immune cells, fibroblasts and a complex extracellular matrix that form the local tumor environment [22].

As described in Tirosh et al. (2016) study, 4645 cells (after filtering out low viability cells) from 19 tumors were captured. After sequencing and normalization, we performed t-distributed stochastic neighbor embedding (t-SNE) to generate a two-dimensional (2D) map of all cells to visualize the transcriptomic landscape. Finally, via k-means clustering, 25 discrete cell clusters were identified (**Figure 1A**). We inferred the cell types of the resulting clusters from the t-SNE analysis by identifying significant genes and compared with the cell marker database (Figure S1; Supplementary File 1). In total, 8 cell types were clustered including ECs (cluster 19 and 22), macrophages (cluster 6), fibroblasts (cluster 17 and 20), melanocytes (cluster 4, 8, 16 and 18), podocytes (cluster 7, 9, 10, 11 and 21), B cells (3, 23, and 24), T cells (cluster 1, 2, 5, 12, 13 and 15) and MTCs (cluster 14 and 25). To further analyze each cell population, another t-SNE map was generated via ASAP (**Figure 1B**). Importantly, when comparing patients, cell clusters in melanoma were highly patient-specific (**Figure 1C** and **1D**). The percent of each main cell cluster in melanoma samples was different. It might suggest different cell constituents lead to various tumor states. Tumors differ from normal tissue often because of the presence of malignant cells. To identify the relation between malignant cells and metastasis, we calculated the percent of malignant cells in each cell population (**Figure 1E** and **1F**). Interestingly, in addition to melanocytes, about 20% of fibroblasts were malignant. It has been reported that fibroblasts could promote the invasion and migration of malignant melanocytes [23]. Thus, we suppose that CAF plays a complementary role in constructing a microenvironment for melanocyte transfer. Because of heterogeneity, the same kind of cells would be clustered into various subtypes. Therefore, greater details of the main cell types should be explored.

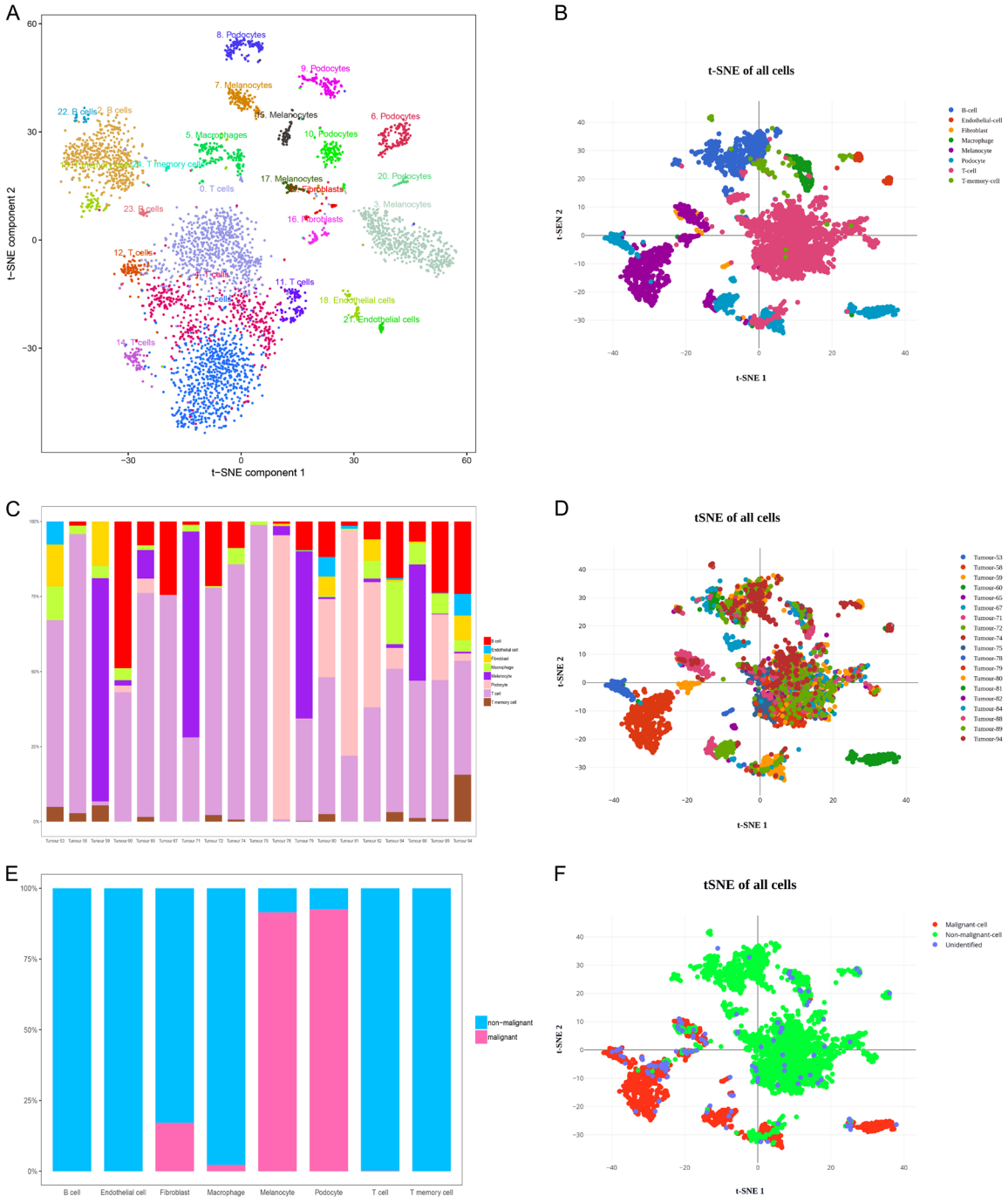


**Figure 1.** The main cell population identified and subpopulation analysis. A. T-SNE projection of 4645 cells from ALONA (each point represents a single cell), labeled with cell lineage. Cells are grouped by colors representing unsupervised clustering results. B. T-SNE projection of all cells from ASAP, colored by cell type. C. The proportion of cells that contributed to each cluster by melanoma sample. D. T-SNE projection of all cells from ASAP, colored by tumor samples. E. Proportions of malignant vs. non-malignant cells of 8 main cell populations. F. T-SNE projection of all cells from ASAP, colored by cell character. t-distributed stochastic neighbor embedding (t-SNE).

*ECs*

ECs line the inner surface of blood vessels and constitute a selective barrier between blood and tissue or tumor and normal tissue. Despite a simple phenotype, ECs play a critical role in a variety of physiological processes, including the maintenance of blood fluidity and immunity

[24]. Unnormal vasculature in tumors might promote cancer development. Tumor ECs regulate several aspects of tumor biology, from delivering oxygen and nutrients to shaping the immune response and providing a barrier against tumor cell metastasis. Targeting tumor ECs represents an important modality in cancer therapy [25]. However, ECs in melanoma are not identical and need a systematized study.

Aggregately 74 ECs were identified with marker genes and executed cluster analysis again via ALONA (**Figure 2A**; Supplementary File 2). 2 clusters (n = 39, n = 35) were distinguished with high expression of a ribosomal protein family. In addition, 183 DEGs (log FC ≥ 2: SPARCL1, IFI27, IFITM1, AQP1, NRP1, COL15A1, RNASE1, SPARC, NOTCH4, DARC, ELTD1, CCL21, NTS, EFEMP1, TFF3, LYVE1, MMRN1, PROX1, DKK3, PDPN, SEMA3A, CXCR7, RBP1 and MFAP2) between 2 clusters were screened (**Figure 2B-D**) followed by pathway and GO enrichment. The most significantly different pathway and GO are hematopoietic cell lineage (pathway, FDR = 0.000465), response to wounding (BP, FDR = 0.000232), extracellular region part (CC, FDR = 7.39E-12) and collagen binding (MF, FDR = 0.00315) respectively (Figure S2). The heterogeneity of cells may be caused by the various states and development of cells. Thus, we performed both state (**Figure 2E**) and pseudotime (**Figure 2E**) trajectory analysis according to the pathway and GO. Through comparing DEG-sets involved in the above pathway and GO, 4 genes (CD34, FN1, PDGFA and SPARC) were associated with more than 3 functions and the expression level of single cells was shown by t-SNE (**Figure 2E**). It has been demonstrated that CD34 immunoreactivity closely parallels both the different morphologic steps of melanoma progression and the presence of aggressive behavior. CD34 might be related to endothelial trans-differentiation of melanoma cells [26]. PDGFA was also verified to influence tumor progress via tumor vasculature [27, 28]. Furthermore, the 16 DEGs (NOTCH4, IL3RA, LAMA5, JAG2, LPAR6, NQO1, FZD4, LAMA4, IL7, FN1, JUP, FLT4, PDGFA, GNG12, TGFA and IGF1) were enriched in pathways in cancer.

Hence, we supposed that different EC subtypes could mediate melanoma via DEG expression profiles. This transcriptional profile of ECs can serve as a reference point for assessing the physiological nature of melanoma.

*CAF*

Among all cells, fibroblasts have strong adaptability and stress tolerance due to their intrinsic survival programs and cellular plasticity. Cancer is associated with fibroblasts at all stages of disease progression. Cancer-associated fibroblasts (CAFs) might synthesize different tumor components that create tumor microenvironments and resistance to chemotherapy. The pleiotropic actions of CAFs in cancer are probably reflective of their heterogeneity and plasticity [29]. CAF can be roughly divided into resting fibroblasts and functional fibroblasts just like T cell differentiation.

In our samples, 105 fibroblasts were detected. Sub clustering revealed three distinct subtypes (n = 47, n = 37 and n = 21). After comparing a single cluster vs. all other cells, 3 DEG sets were identified and shown by heatmap (**Figure 3A-D**; Supplementary File 3). Function enrichment analysis for each DEG-set was performed and obtain the intersection items via overlaying (Figure S3). Finally, focal adhesion, extracellular structure organization, vacuolar part and integrin binding were selected to process trajectory analysis as described above (**Figure 3E**). Each function could involve some DEGs, whose occurrence numbers greater than average were defined as hub genes. For example, integrin subunit alpha 5 (ITGA5), produces an integrin alpha chain that functions in cell surface adhesion and tumor invasion [32]. Decorin (DCN), as an important component of the extracellular matrix (ECM), is a small leucine-rich proteoglycan and synthesized by fibroblasts. It has been reported in renal cell carcinoma, DCN was decreased in cancerous tissues and highly correlated to tumor size [33]. In addition, matrix metalloproteinase 2 (MMP-2) [34] and glycoprotein non-metastatic B (GPNMB) [35] from CAF were also confirmed to influence tumor cell invasion and metastasis.

CAFs participate in tumorigenesis, metastasis, metabolism, immunity, and can function as positive or negative regulators of tumor growth [36-39]. Therefore, the analysis of CAF heterogeneity provides a point of reference for examining the role of CAFs subsets in the establishment and progression of melanoma.

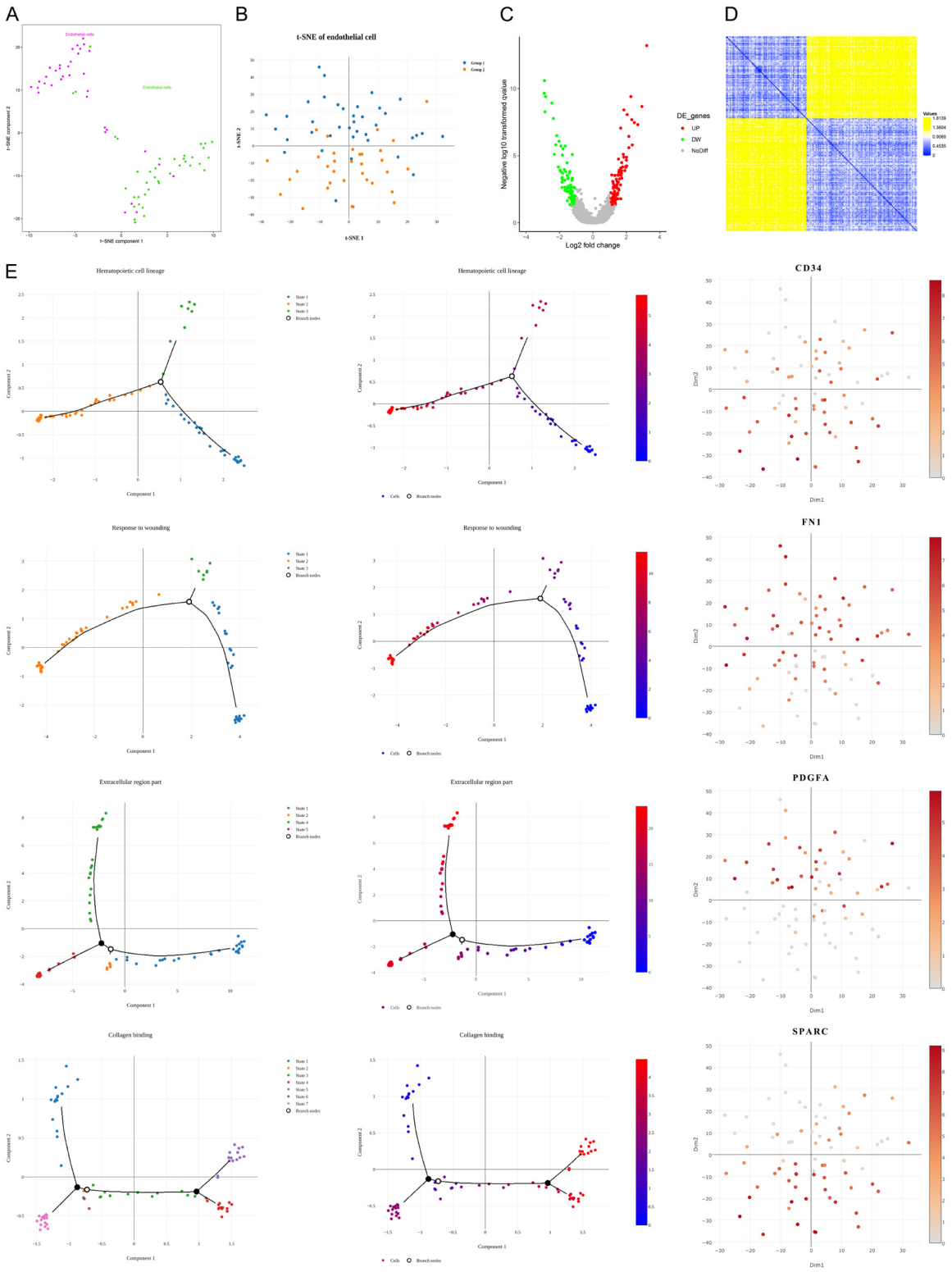


**Figure 2.** The clustering and characteristic description of EC subtypes. A and B. The t-SNE plots of 74 ECs generated from ALONA and ASAP were colored by subtypes. C. The volcano plot of DEGs (G 1 vs. G 2), each dot represents a gene. The gray ones represent genes without significant difference while the green and red ones represent decreased and increased genes in group 1, respectively. D. The heatmap of DEGs, the legend for relative expression from lowest expression (blue) to highest expression (yellow) (top right). E. The first two columns are trajectory analysis of ECs based on hematopoietic cell lineage (pathway), response to wounding (BP), extracellular region part (CC) and collagen binding (MF). The last column showed expression of 4 specific genes (CD34, FN1, PDGFA and SPARC) via t-SNE. The legends represent different states and levels locate at right. t-distributed stochastic neighbor embedding (t-SNE), differently expressed genes (DEGs).

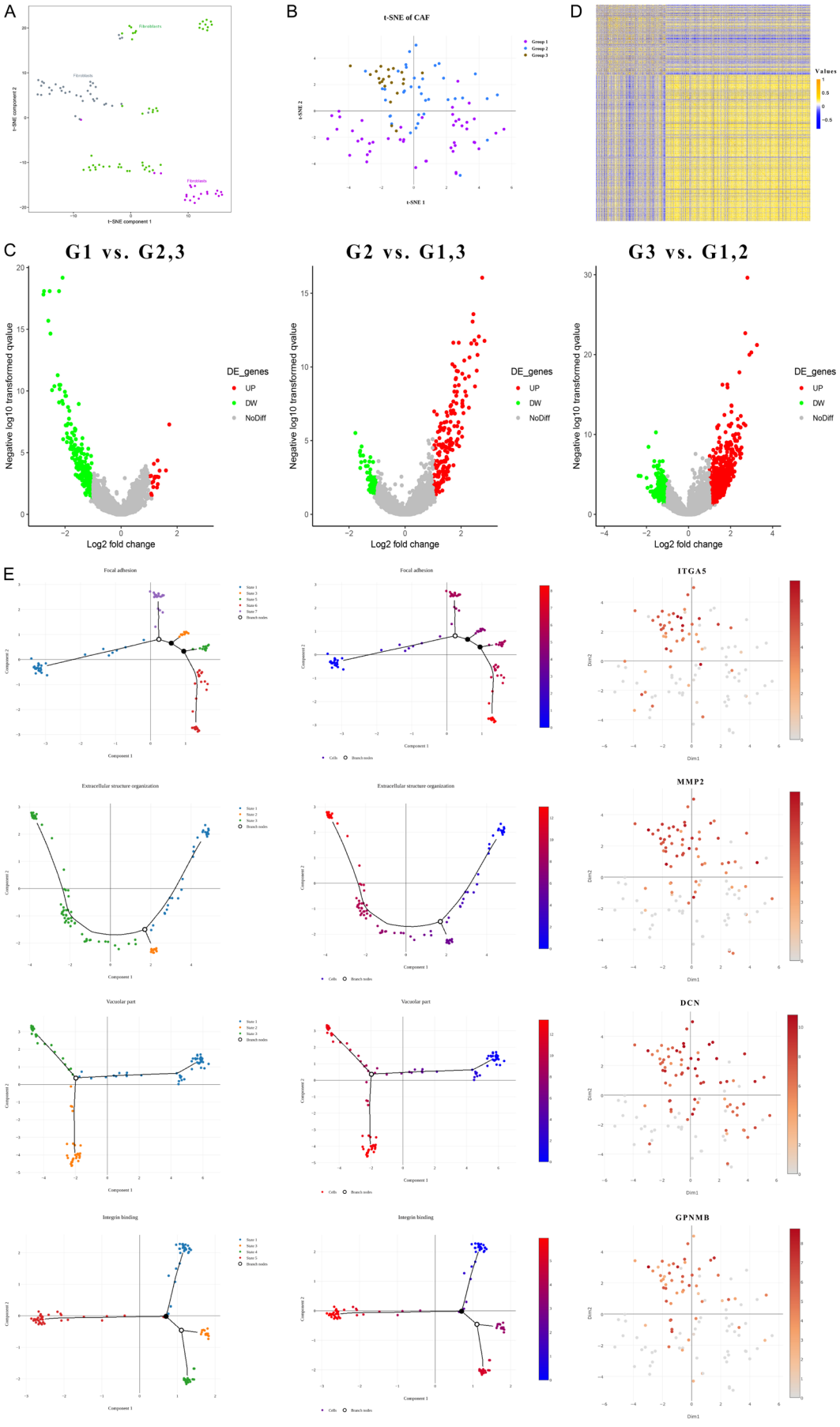
A
Fibroblasts
Fibroblasts
Fibroblasts
t-SNE component 1
t-SNE component 2
B
t-SNE of CAF
Group 1
Group 2
Group 3
t-SNE 1
t-SNE 2
D
Values
C
G1 vs. G2,3
G2 vs. G1,3
G3 vs. G1,2
Negative log10 transformed qvalue
Log2 fold change
DE_genes
UP
DW
NoDiff
E
Focal adhesion
Extracellular structure organization
Vacuolar part
Integrin binding
ITGA5
MMP2
DCN
GPNMB

**Figure 3.** The clustering and characteristic description of CAF subtypes. A and B. The t-SNE plots of 105 CAFs generated from ALONA and ASAP were colored by subtypes. C. The volcano plots of DEGs (G 1 vs. G 2, 3; G 2 vs. G 1, 3 and G 3 vs. G 1, 2), each dot represents a gene. The gray ones represent genes without significant difference while the green and red ones represent decreased and increased genes in each group respectively when compared with other CAFs. D. The heatmap of DEGs, the legend for relative expression from lowest expression (blue) to highest expression (yellow) (top right). E. The first two columns are trajectory analysis of CAFs based on focal adhesion (pathway), extracellular structure organization (BP), vacuolar part (CC) and integrin binding (MF). The last column showed expression of 4 specific genes (ITGA5, MMP2, DCN and GPNMB) via t-SNE. The legends represent different states and levels locate at right. t-distributed stochastic neighbor embedding (t-SNE), differently expressed genes (DEGs).

**Table 1.** Characteristic markers of M1 and M2 macrophages

| Cell type | Recognized markers | References |
|---|---|---|
| M1 macrophages | CD80+, CD86+, TNF-α, VEGF, SOCS3, CCR7 | [72-77] |
| M2 macrophages | CD163, IL-10, SOSC1/2, CD206, CCL-18, PDGF-BB, MMP | [77-80] |

*Macrophage*

Macrophages are widely distributed innate immune cells that play indispensable roles in promoting tumor angiogenesis, growth, metastasis, and immunosuppression through secreting cytokines, chemokines, and proteases. Macrophages can be activated by an abundance of stimuli and polarized into 2 distinct subsets, classically activated (M1) and alternatively activated (M2) macrophages [40]. The particular markers for all subtypes of macrophages were listed in **Table 1**. In most tumors, the infiltrated macrophages are considered to be of the M2 phenotype, which provides an immunosuppressive microenvironment for tumor growth. However, as reported recently, macrophages in the tumor have a special transition period from M1 to M2 phenotype, which suggests there is another phenotype in the whole tumor progression.

In our study, 3 types were clustered via recognizing difference transcriptome and shown with t-SNE maps (**Figure 4A** and **4B**; Supplementary File 4). There are 95, 93 and 52 DEGs in cluster 1, 2 and 3, respectively compared with other cells. After function enrichment and intersection (Figure S4), NF-κB signaling pathway, immune effector process, extracellular space and heparin binding were the most significant different functions among 3 macrophage types. Besides, it was found that tumor necrosis factor alpha-induced protein 3 (TNFAIP3), interleukin-1β (IL1B), interleukin 1 receptor antagonist (IL1RN) and SELL are the most frequent genes in these functions. TNFAIP3, an anti-inflammatory protein implicated in multiple autoimmune and regulated by NF-κB, has been demonstrated that dysregulated expression may be a contributor to excessive inflammatory responses [41]. IL1B is abundant in the tumor microenvironment, where this cytokine can promote tumor growth, but also antitumor activities. IL-1B could mediate the recruitment and differentiation of inflammatory monocytes like macrophages. Furthermore, it has been verified that IL1B from M2 macrophages promotes migration and invasion of esophageal squamous cell carcinoma enhancing epithelial-mesenchymal transition and activating NF-κB signaling pathway [42]. Besides, IL1RN was reported to promote macrophage polarization [43] and SELL was considered as pro-inflammatory mediators like IL-1B [44] (**Figure 4C-E**).

*B cells*

B cells represent 15-20% of all infiltrating lymphocytes, besides, it was confirmed that in thicker tumors and primary melanomas, B cell was recruited and associated with a lower risk of metastasis and longer survival [45-48]. Analysis of 329 melanoma specimens obtained from TCGA showed that patients with the high immune response not only contain infiltrative T cells, B cells were also detected [49]. In addition, patient-derived B cells can kill melanoma cells in vitro by antibody dependent cellular cytotoxicity (ADCC) [50]. However, in the tumor immune microenvironment, each B cell cluster might play a distinct role in different tumor stages. Thus, studying the variation of gene expression and functions between B cell clusters is necessary.

As the same analysis pipeline above, 5 subtypes were identified. Interestingly, just No.5

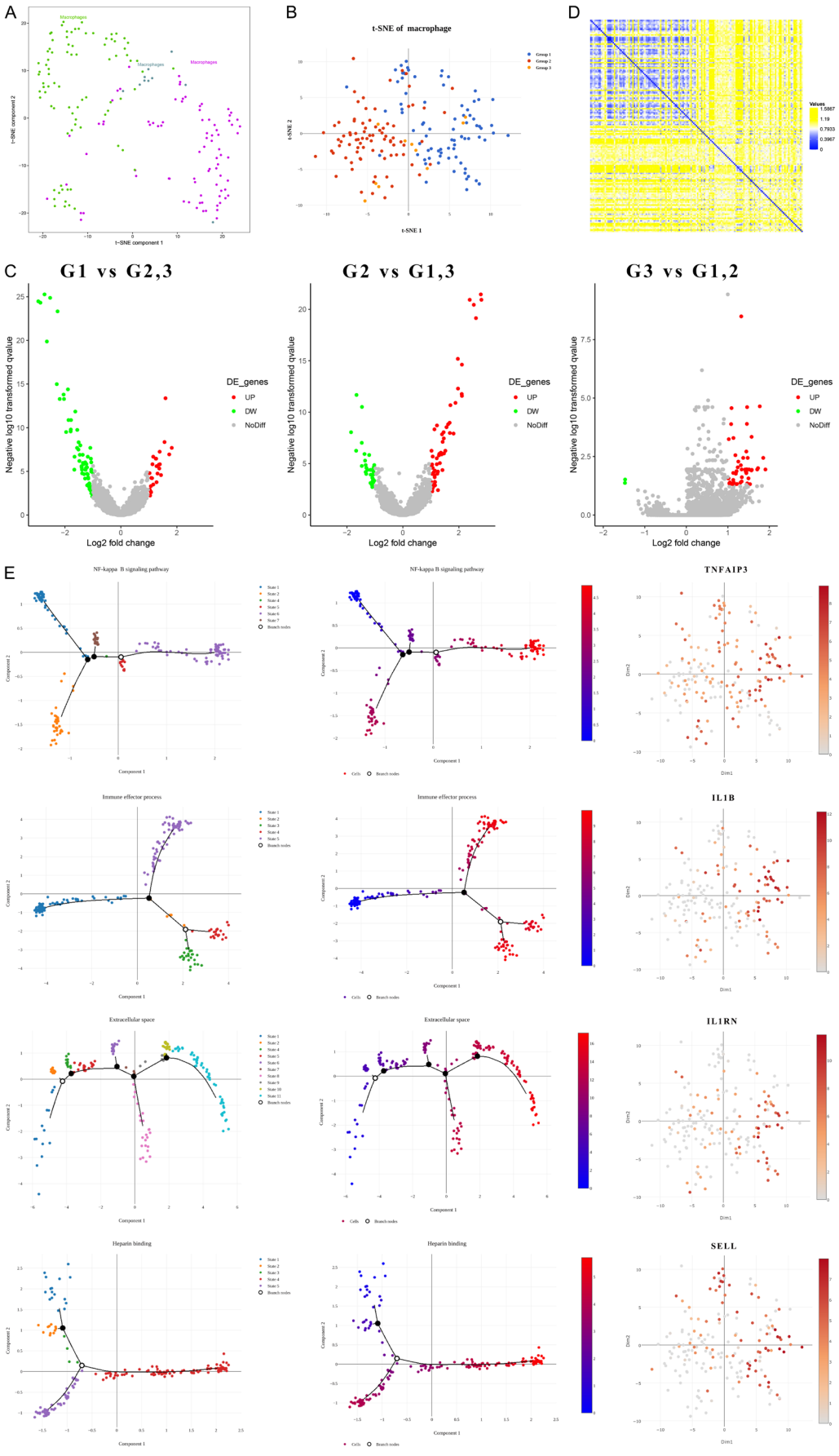
A
Macrophages
Macrophages
Macrophages
t-SNE component 2
t-SNE component 1
B
t-SNE of macrophage
Group 1
Group 2
Group 3
t-SNE 2
t-SNE 1
D
Values
1.5867
1.19
0.7933
0.3967
0
C
G1 vs G2,3
G2 vs G1,3
G3 vs G1,2
Negative log10 transformed qvalue
Log2 fold change
DE_genes
UP
DW
NoDiff
E
NF-kappa B signaling pathway
TNFAIP3
Immune effector process
IL1B
Extracellular space
IL1RN
Heparin binding
SELL
Component 1
Component 2
Dim1
Dim2
Cells
Branch nodes

**Figure 4.** The clustering and characteristic description of macrophage subtypes. A and B. The t-SNE plots of 179 macrophages generated from ALONA and ASAP were colored by subtypes. C. The volcano plots of DEGs (G 1 vs. G 2, 3; G 2 vs. G 1, 3 and G 3 vs. G 1, 2), each dot represents a gene. The gray ones represent genes without significant difference while the green and red ones represent decreased and increased genes in each group respectively when compared with other macrophages. D. The heatmap of DEGs, the legend for relative expression from lowest expression (blue) to highest expression (yellow) (top right). E. The first two columns are trajectory analysis of macrophages based on the NF-kappa B signaling pathway (pathway), immune effector process (BP), extracellular space (CC) and heparin binding (MF). The last column showed expression of 4 specific genes (TNFAIP3, IL1B, IL1RN and SELL) via t-SNE. The legends represent different states and levels locate at right. t-distributed stochastic neighbor embedding (t-SNE), differently expressed genes (DEGs).

cluster appeared DEGs (152 down-regulated genes and 582 up-regulated genes) when compared with other cells (**Figure 5A-D**; Supplementary File 5; Figure S5). We speculated the basis of clustering may depend on the appearance of marker genes, not expression level. All DEGs were enriched in 42 pathways (protein processing in endoplasmic reticulum), 120 BP items (Protein N-linked glycosylation), 68 CC items (Organelle membrane) and 29 MF items (Oxidoreductase activity, acting on NAD(P)H) (Figure S6). Through trajectory analysis based on the most enriched functions, all B cells could be divided into various state levels (**Figure 5E**). According to the occurrence frequency of DEGs in enriched function, 4 significant genes (i.e. EDEM1, LMAN1, CALR and NDUFA1) were shown with t-SNE. Nevertheless, scarcely any studies were searched and the mechanism should be further explored.

*T cell*

T lymphocytes have a major role in the antitumor immune responses and are the dominant elements in the tumor microenvironment. A total of 2250 cells were recognized as T lymphocytes, the largest population in our study. Go through clustering, 7 communities were identified which belong to 3 subtypes (T cell: cluster 1 and 5; T memory cell: cluster 2, 3, 4 and 7; NK cell: cluster 6) (**Figure 6A-C**; Supplementary File 6). Each cluster was compared with other T cells, DEGs were screened (**Figure 6D**). Remarkably, only 40 down-regulated genes (Top 10: LSP1, IL2RG, TPI1, NKG7, RAC2, ATP5B, TAP1, RHOA, CD27 and ALDOA) were detected in cluster 3 while in cluster 4, only 14 up-regulated genes (Top 10: PMEL, CD63, CST3, APOE, HSPB1, GPNMB, PRAME, TYR, ANXA5 and WARS) were identified (**Figure 7C**). It suggested that cluster 3 or 4 may just exhibit loss or addition of functions, respectively. Each DEG set performed function enrichment analysis (Figure S7). The antigen processing and presentation pathway were enriched in cluster 1, 2, 3, 5 and 7, not in cluster 6 (NK cell). The cell activation and cell surface were enriched in cluster 1, 2, 3, 4, 6 and 7, not in cluster 5 (T cell). The cytokine receptor activity was enriched in cluster 1, 2, 3, 6 and 7, not in cluster 4 and 5 (T memory cell and T cell). In addition, the functions of DEGs among 3 main subtypes were also enriched (Figure S8). There are 89,104 and 57 DEGs in NK cell vs. T cell, NK cell vs. T memory cell and T cell vs. T memory cell comparisons, respectively.

T cells, the largest group in our study act as an important part of tumor immunity. Once receiving antigen signal, the differentiation into T cell subtypes with specific functions is very complex. Thus, trajectory analysis depends on important functions were performed and the T cells were divided according to the cell state or pseudotime (**Figure 6E**). Similarly, 4 genes (CD4, TIGIT, HLA-DRB1 and IL2RB) with the most frequency were shown by t-SNE. CD4, a membrane glycoprotein of T lymphocytes that could interact with major histocompatibility complex class II (MHC-II) antigens and initiate or augment the early phase of T-cell activation [53]. TIGIT, is an inhibitory receptor expressed in activated T cells, Tregs, and NK cells. It was determined that TIGIT was upregulated and regulated the expansion and function of tumor-infiltrating CD8+ T cells in melanoma patients, associated with programmed cell death protein 1 (PD-1) [54]. HLA-DRB1 and IL2RB were also confirmed to take part in T cell-mediated immune response [55] while the detailed molecular mechanisms were still covered.

*MTCs*

Immunogenicity of human malignant melanoma is well documented, including antigen identification of melanoma and spontaneous tumor

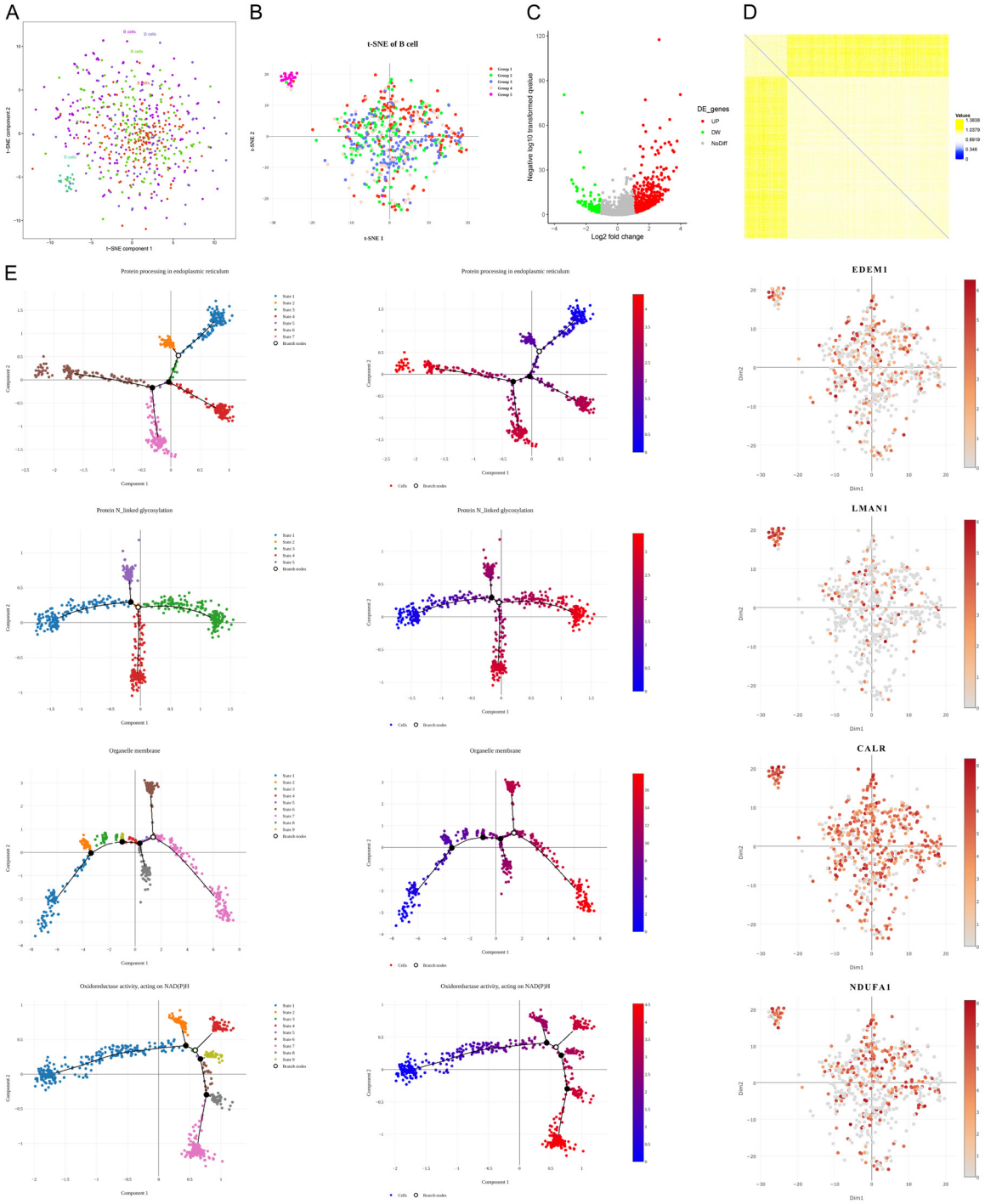


**Figure 5.** The clustering and characteristic description of B cell subtypes. A and B. The t-SNE plots of 597 B cells generated from ALONA and ASAP were colored by subtypes. C. The volcano plots of DEGs (G 5 vs. G 1, 2, 3 and 4), each dot represents a gene. The gray ones represent genes without significant difference while the green and red ones represent decreased and increased genes respectively. D. The heatmap of DEGs, the legend for relative expression from lowest expression (blue) to highest expression (yellow) (top right). E. The first two columns are trajectory analysis of B cells based on protein processing in the endoplasmic reticulum (pathway), protein N-linked glycosylation (BP), organelle membrane (CC) and oxidoreductase activity, acting on NAD(P)H (MF). The last column showed expression of 4 specific genes (EDEM1, LMAN1, CALR and NDUFA1) via t-SNE. The legends represent different states and levels locate at right. t-distributed stochastic neighbor embedding (t-SNE), differently expressed genes (DEGs).

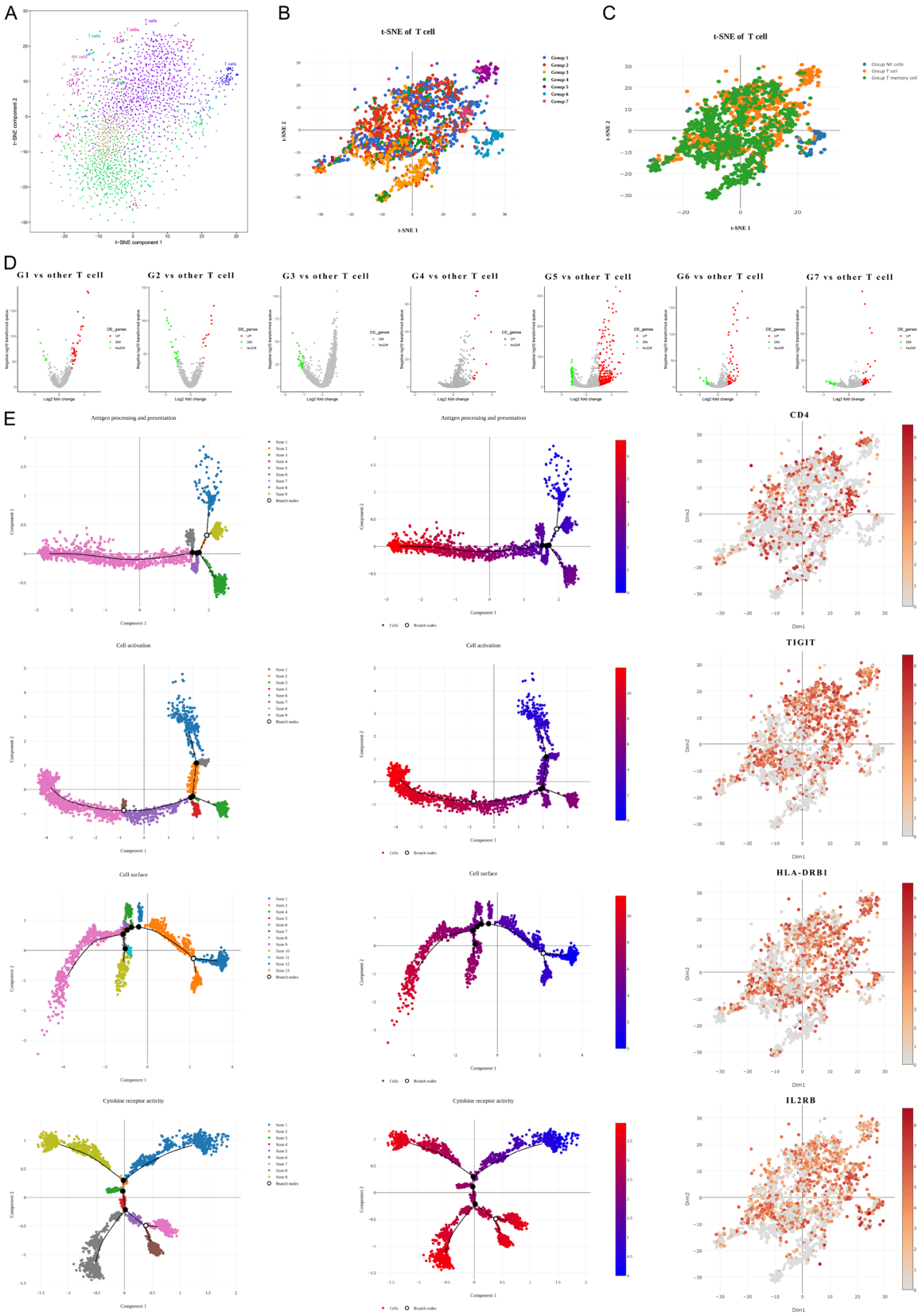


**Figure 6.** The clustering and characteristic description of T cell subtypes. A-C. The t-SNE plots of 2250 T cells generated from ALONA and ASAP were colored by subtypes. D. The volcano plots of DEGs in each group when compared with other T cells, each dot represents one gene. The gray ones represent genes without significant difference while

the green and red ones represent decreased and increased genes. E. The first two columns are trajectory analysis of T cells based on antigen processing and presentation (pathway), cell activation (BP), cell surface (CC) and cytokine receptor activity (MF). The last column showed expression of 4 specific genes (CD4, TIGIT, HLA-DRB1 and IL2RB) via t-SNE. The legends represent different states and levels locate at right. t-distributed stochastic neighbor embedding (t-SNE), differently expressed genes (DEGs).

regressions thereby providing convictive evidence for T cells induced antitumor immunity [56, 57]. The presence of tumor-antigen stimulates naive T cells to differentiate into memory and effector T cells to eliminate abnormal cells. In this respect, antigen-specific memory T cells are significant because they are known to react to antigens faster and stronger than naive T cells by increased proliferation. In addition, they release a broader spectrum of cytokines and need less co-stimulation by particular antigen presenting cells [58-60]. While surgery currently remains the primary cure for solid tumors, memory T cell responses may be required for the durable prevention of tumor recurrence and metastasis following excision [61]. Traditionally, tumor-infiltrating T memory cells could also be divided into 2 subtypes (i.e. CD8+ and CD4+), also 3 types (i.e. central memory T cells, effector memory T cells and migratory memory T cells), and sufficiently suggested heterogeneity of memory T cell.

A total of 101 memory T cells were clustered into 3 populations via ALONA (**Figure 7A** and **7B**; Supplementary File 7). After pairwise comparison, 3 DEG sets were executed function enrichment analysis (Figure S9). Furthermore, 11 pathways (apoptosis), 33 BPs (apoptotic process), 12 CCs (external side of plasma membrane) and 5MFs (cysteine-type endopeptidase regulator activity involved in the apoptotic process) were enriched from 3 DEG sets simultaneously (**Figure 7D**). It may suggeste the developmental trajectory of 3 subtypes was strongly associated with apoptosis. By trajectory analysis (state and pseudotime), the differentiation nodes and classified clusters were detected. 4 DEGs (TNFRSF1A, CDKN1A, MS4A1 and TNFAIP3) with the most frequency in above functions were shown by t-SNE. However, the evidence that could support these four genes' immune role in melanoma is scarce (**Figure 7E**).

Currently, diagnosis, prognosis and therapy of melanoma are based on the TNM staging system, which includes clinic-pathological factors: tumor thickness, ulceration, mitotic rate, sentinel lymph node status and metastases [62]. However, traditional classification cannot diagnose the distinct progression and precise treatments may not be found. It implied the new parameters that stratify tumor state accurately was urgently needed. Profound evaluation of tumor immune cells can enlighten the way to new and effective solutions for melanoma patients.

*Melanocytes and podocytes*

Although various cell clusters like endothelial cells, CAFs and immune cells contribute to the tumor microenvironment formation, the main cause of melanoma is melanocyte variation. However, the cancer cells in melanoma also present heterogeneous phenotypes and result in different abilities of invasion and drug resistance. Hence, analyzing the differences between melanocyte groups could provide a new and comprehensive view of melanoma.

Firstly, follow in the regular analysis process, 764 melanocytes were clustered into 6 groups and the DEGs of each group were shown by volcano plots and heatmaps (**Figure 8A-D**; Supplementary File 8). After enrichment analysis, trajectory analysis based on ECM-receptor interaction, negative regulation of the apoptotic process, cytoplasmic vesicle part and enzyme inhibitor activity were performed (**Figures 8E** and S10). Interestingly, it was found that lots of enriched CC items were associated with vesicles, which may science the active metabolism in cancer cells. The expression of 4 genes (ITGA3, ANXA1, CD9 and SERPINA1) with the most frequency was shown by t-SNE maps. In addition, according to the clinical data of 479 melanoma patients from TCGA, the survivorship curve (overall survival and disease-free survival) was calculated. The results suggested that either ANXA1 or SERPINA1 with low levels would increase the risk of poor prognosis (**Figure 8F**). Moreover, through comparing with the t-SNE map colored by tumor samples (Figure S11), it was found that only in tumor 79, 3 subtypes (cluster 1, 2 and 3) were identified and these 4 genes were expressed with higher levels. Notably, ITGA3, ANXA1 and CD9 were

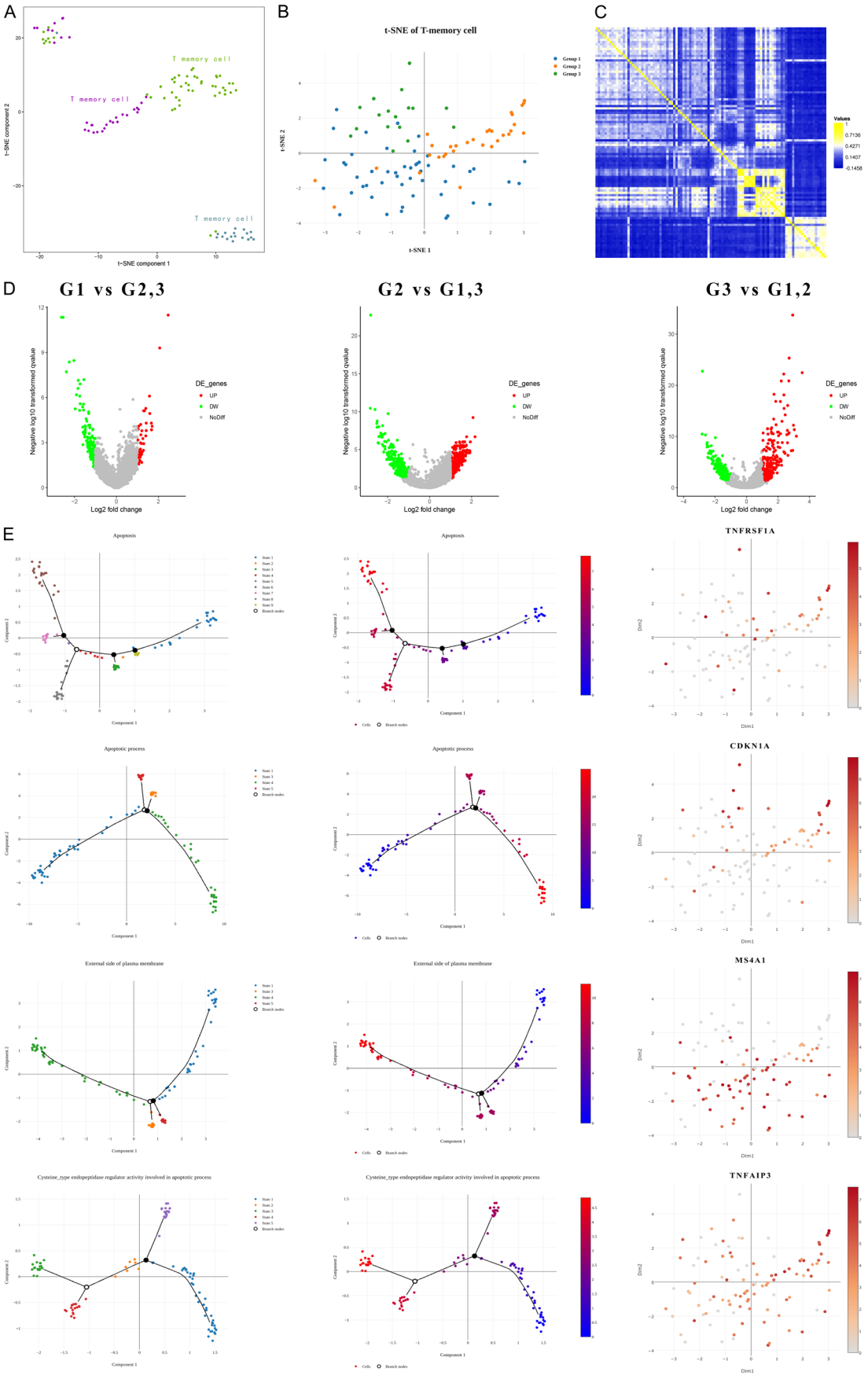
A
T memory cell
T memory cell
T memory cell
t-SNE component 1
t-SNE component 2
B
t-SNE of T-memory cell
Group 1
Group 2
Group 3
t-SNE 1
t-SNE 2
C
Values
D
G1 vs G2,3
G2 vs G1,3
G3 vs G1,2
Negative log10 transformed qvalue
Log2 fold change
DE_genes
UP
DW
NoDiff
E
Apoptosis
TNFRSF1A
Apoptotic process
CDKN1A
External side of plasma membrane
MS4A1
Cysteine_type endopeptidase regulator activity involved in apoptotic process
TNFAIP3
Component 1
Component 2
Dim1
Dim2
Cells
Branch nodes

**Figure 7.** The clustering and characteristic description of memory T cell subtypes. A and B. The t-SNE plots of 101 memory T cells generated from ALONA and ASAP were colored by subtypes. C. The volcano plots of DEGs (G 1 vs. G 2, 3; G 2 vs. G 1, 3 and G 3 vs. G 1, 2), each dot represents a gene. The gray ones represent genes without significant difference while the green and red ones represent decreased and increased genes in each group respectively when compared with other memory T cells. D. The heatmap of DEGs, the legend for relative expression from lowest expression (blue) to highest expression (yellow) (top right). E. The first two columns are trajectory analysis of memory T cells based on apoptosis (pathway), apoptotic process (BP), external side of plasma membrane (CC) and cysteine-type endopeptidase regulator activity involved in the apoptotic process (MF). The last column showed expression of 4 specific genes (TNFRSF1A, CDKN1A, MS4A1 and TNFAIP3) via t-SNE. The legends represent different states and levels locate at right. t-distributed stochastic neighbor embedding (t-SNE), differently expressed genes (DEGs).

verified to influence melanoma invasion [63-65]. Even though no evidence proven the role of SERPINA1 in melanoma, it has been confirmed that SERPINA1 could promote tumor progression and predict prognosis in colorectal cancer [66].

Because the largest danger of melanoma is malignant invasion, exploring the potential mechanism of malignancy may be the most fundamental task. According to Itay Tirosh's research [9], all melanocytes were divided into 3 populations, malignant type, non-malignant type and unresolved type (Figure S12). In total, 6 down-regulated and 56 up-regulated genes were screened in malignant melanocytes compared with non-malignant ones. Analyzing in TCGA, the mutation rate of 19 genes (down-regulated: PHGDH and RNF19A; up-regulated: DUSP23, SHC1, CSRP1, HAX1, TMED3, SUPT4H1, HIST2H2AA3, SERING3, CTSA, CCDC47, S100A13, LGALS3BP, RPN2, CD164, XRCC6, LAGLS1 and SARAF) were more than 10% (**Figure 9A**). By calculating the survival curve of mutant genes, only 5 genes (PHGDH, RNF19A, CD164, CSRP1 and LAGLS1) have a significant difference between high and low expression levels (**Figure 9B** and **9C**). From The Human Protein Atlas, immunohistochemical photographs of normal tissue and melanoma were obtained. These results further confirmed the expression trend of these 5 genes (**Figure 9D** and **9E**). Moreover, there were no DEGs in the unresolved group when compared with either malignant type or non-malignant type may because this group is in transition from non-malignant to malignant.

Normally, podocytes could be found in the kidney and maintain the glomerular filtration barrier [67]. However, it was detected in our analysis, which may be due to the unspecific markers causing "illusion". By further predictions, it was supposed to be a melanocyte and some basal cells (**Figure 10A** and **10B**; Supplementary File 9). The DEGs from all 6 clusters were performed enrichment analysis and the most significant functions (i.e. cell adhesion molecules, pigment biosynthetic process, cytoplasmic vesicle and identical protein binding) were also used to do trajectory analysis (**Figures 10C-E**, S13). Notably, the pigment biosynthetic process which was enriched in 6 sub-clusters further confirmed that most podocytes were neglected melanocytes. Nevertheless, these "possible" melanocyte clusters may be different from the "true" melanocyte groups in some ways need further research.

## Discussion

Melanoma is one of the immunogenic skin cancer with complex ecosystems and is often associated with drug resistance causing poor curative effect. We speculated that these phenomena might be due to the cell heterogeneity in the tumor microenvironment. Thus, 4645 cells extracted from 19 melanoma samples were clustered and studied by function enrichment and trajectory analyses. A total of 8 cell types were identified and immune cells (179 macrophages, 597 B cells, 2250 T cells and 101 T memory cells) occupied the maximum ratio. Strangely, dendritic cells (DCs), professional antigen-presenting cells with a crucial role in the induction of antitumor responses were not detected in our clustering. In Nedelcu et al.'s study, the immunohistochemical study revealed that DCs are more frequent in tumor regressed areas, compared with non-regressed ones like the samples in our study [68]. Hence, we summarized 2 possible causes that result in DCs disappearance. On the one hand, when cells were sorted by flow cytometry, DCs were ignored because of the marker genes and the resolution. In addition, filtering and normalization may also cause data loss. On the other hand, with melanoma development and

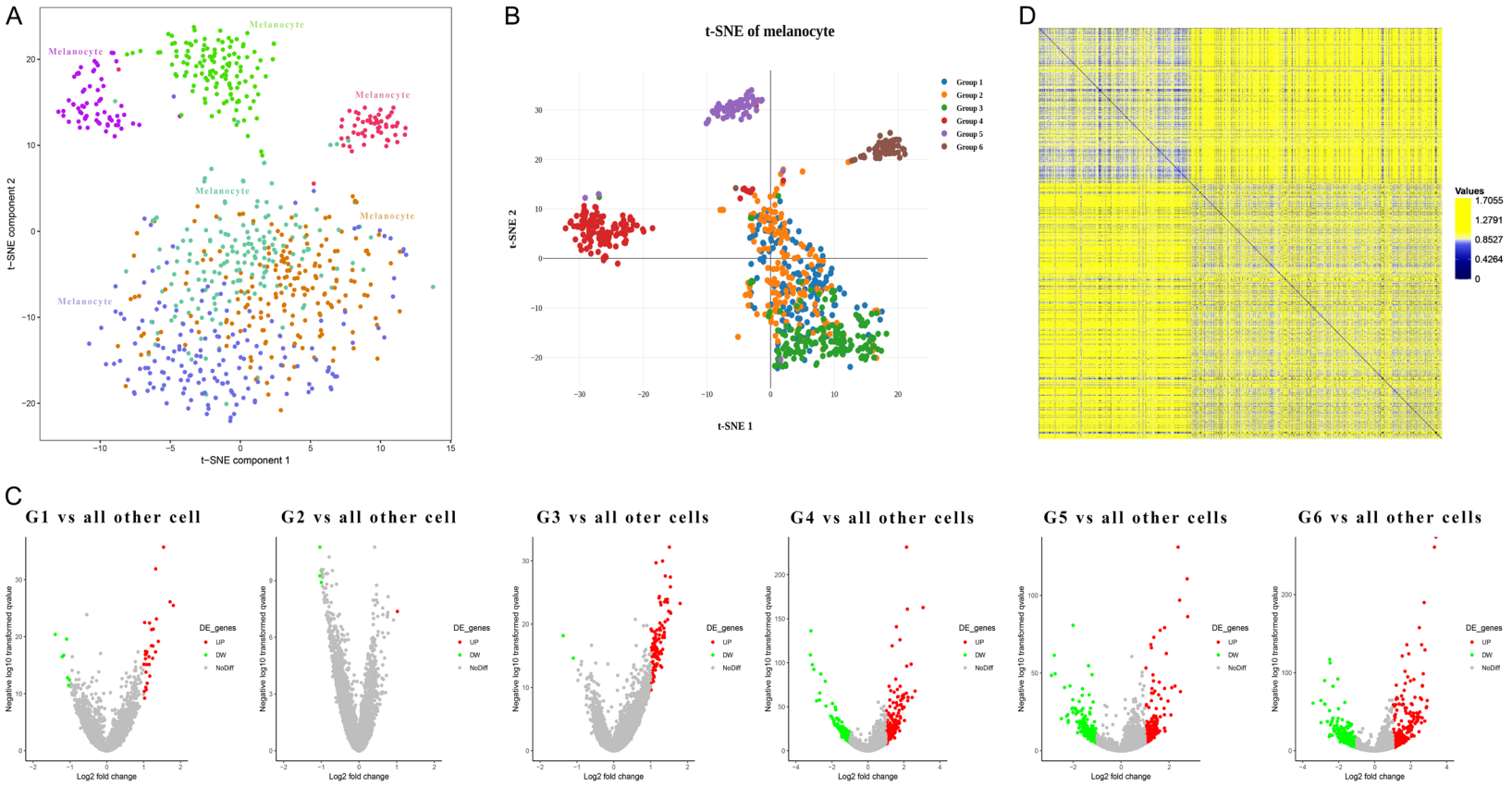
A
Melanocyte
Melanocyte
Melanocyte
Melanocyte
Melanocyte
Melanocyte
t-SNE component 2
t-SNE component 1
B
t-SNE of melanocyte
Group 1
Group 2
Group 3
Group 4
Group 5
Group 6
t-SNE 2
t-SNE 1
D
Values
1.7055
1.2791
0.8527
0.4264
0
C
G1 vs all other cell
G2 vs all other cell
G3 vs all oter cells
G4 vs all other cells
G5 vs all other cells
G6 vs all other cells
Negative log10 transformed qvalue
Log2 fold change
DE_genes
UP
DW
NoDiff

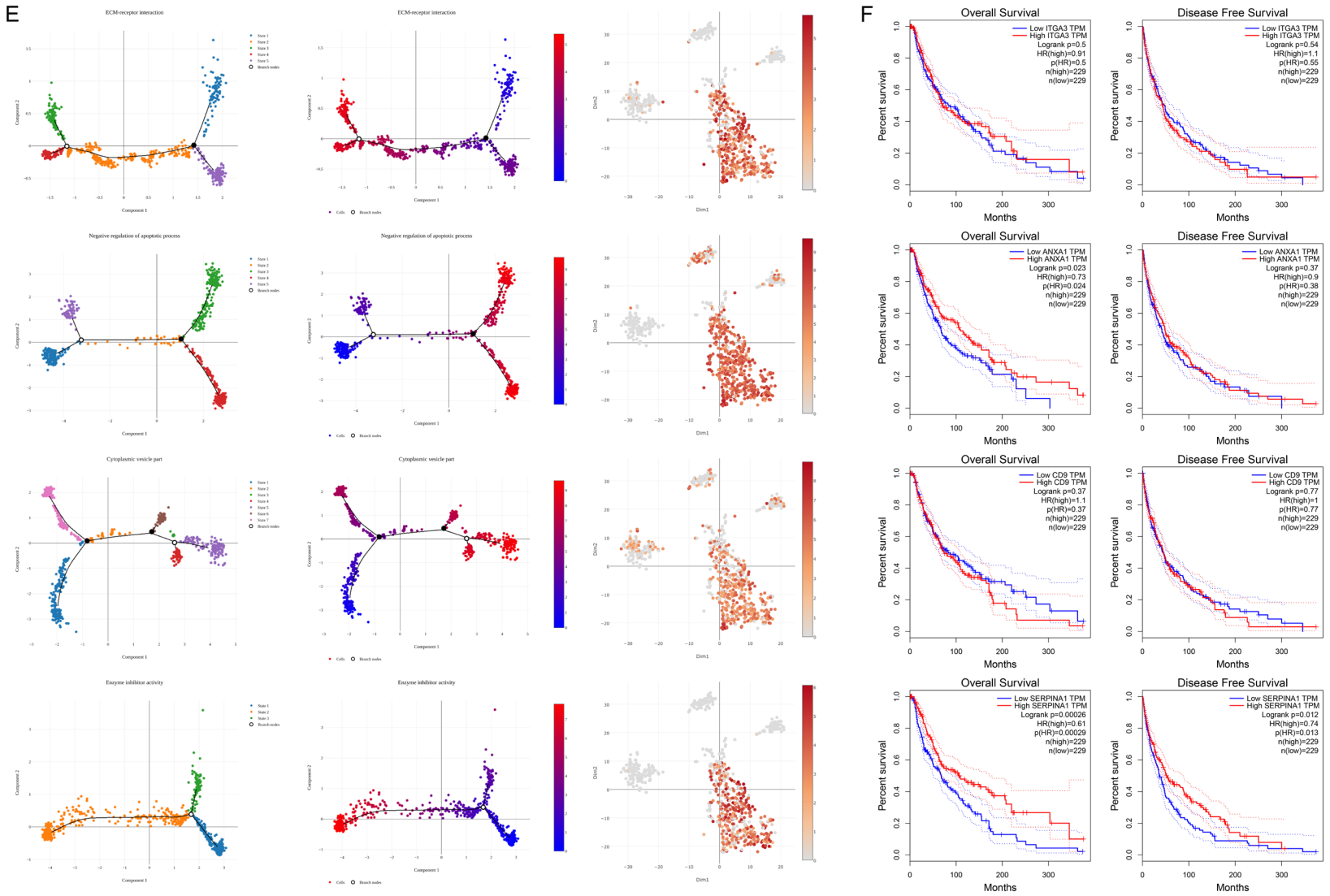


**Figure 8.** The clustering and characteristic description of melanocyte subtypes. A and B. The t-SNE plots of 764 melanocytes generated from ALONA and ASAP were colored by subtypes. C. The volcano plots of DEGs in each group when compared with other melanocytes, each dot represents a gene. The gray ones represent genes without significant difference while the green and red ones represent decreased and increased genes in each group respectively when compared with other melanocytes. D. The heatmap of DEGs, the legend for relative expression from lowest expression (blue) to highest expression (yellow) (top right). E. The first two columns are trajectory analysis of melanocytes based on ECM-receptor interaction (pathway), negative regulation of apoptotic process (BP), cytoplasmic vesicle

part (CC) and enzyme inhibitor activity (MF). The last column showed expression of 4 specific genes (ITGA3, ANXA1, CD9 and SERPINA1) via t-SNE. The legends represent different states and levels locate at right. F. The curves of overall survival and disease-free survival about above 4 genes were calculated based on TCGA. t-distributed stochastic neighbor embedding (t-SNE), differently expressed genes (DEGs), The Cancer Genome Atlas (TCGA).

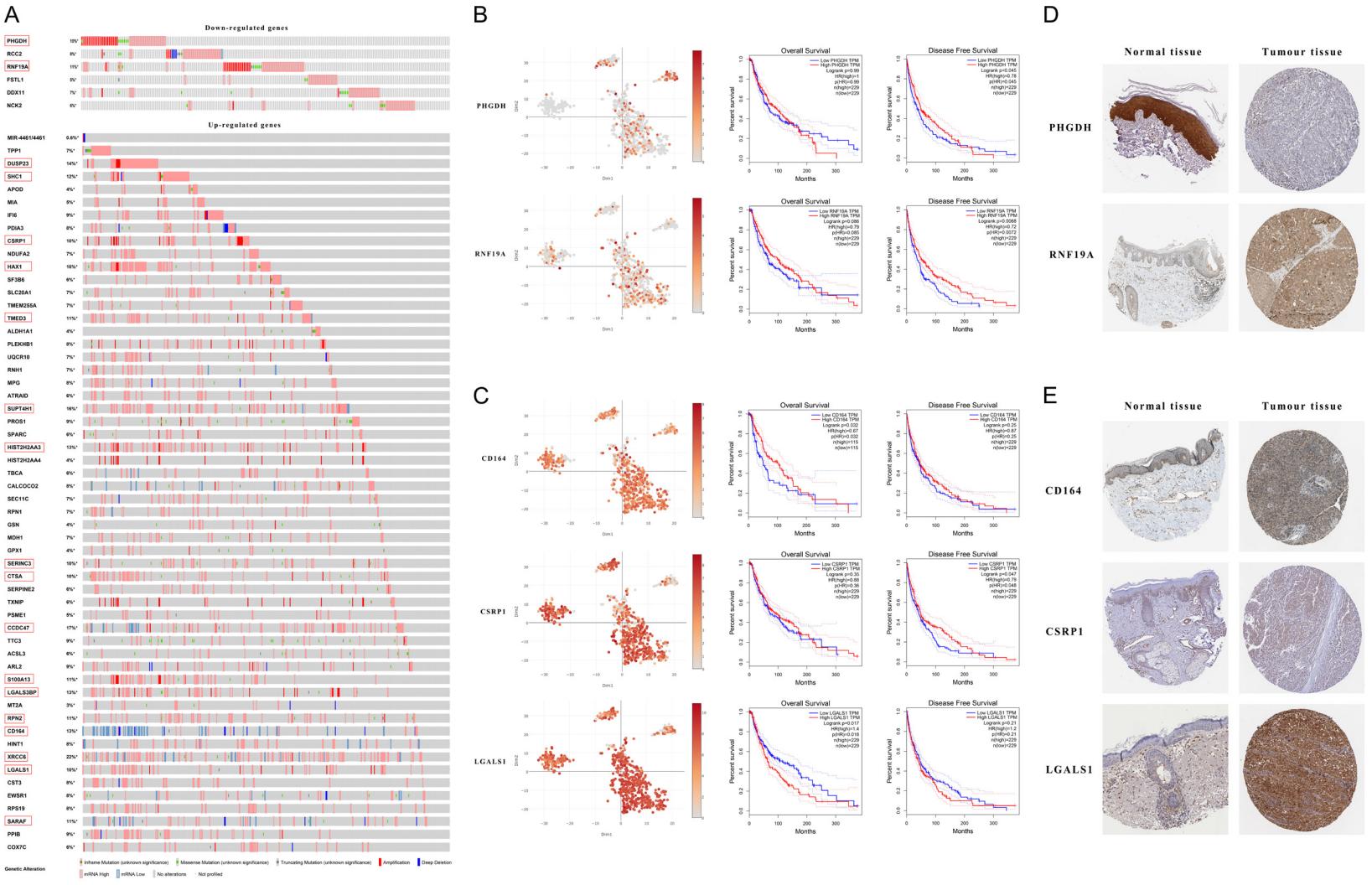

**Figure 9.** The DEGs of malignant melanocytes vs. non-malignant melanocytes. A. Panoramic map of DEGs' mutation in 479 melanoma patients from TCGA. Different colored markers represent different mutation types and the mutation rates of DEGs were list on left. The gene with more than 10% mutation was marked by a red box. B and C. The expression level of DEGs (PHGDH, RNF19A, CD164, CSRP1 and LGALS1) in each melanocyte and the curves of overall survival and disease-free survival were calculated. D and E. The immunohistochemical results of DEGs from normal and tumor tissues. differently expressed genes (DEGs), The Cancer Genome Atlas (TCGA).

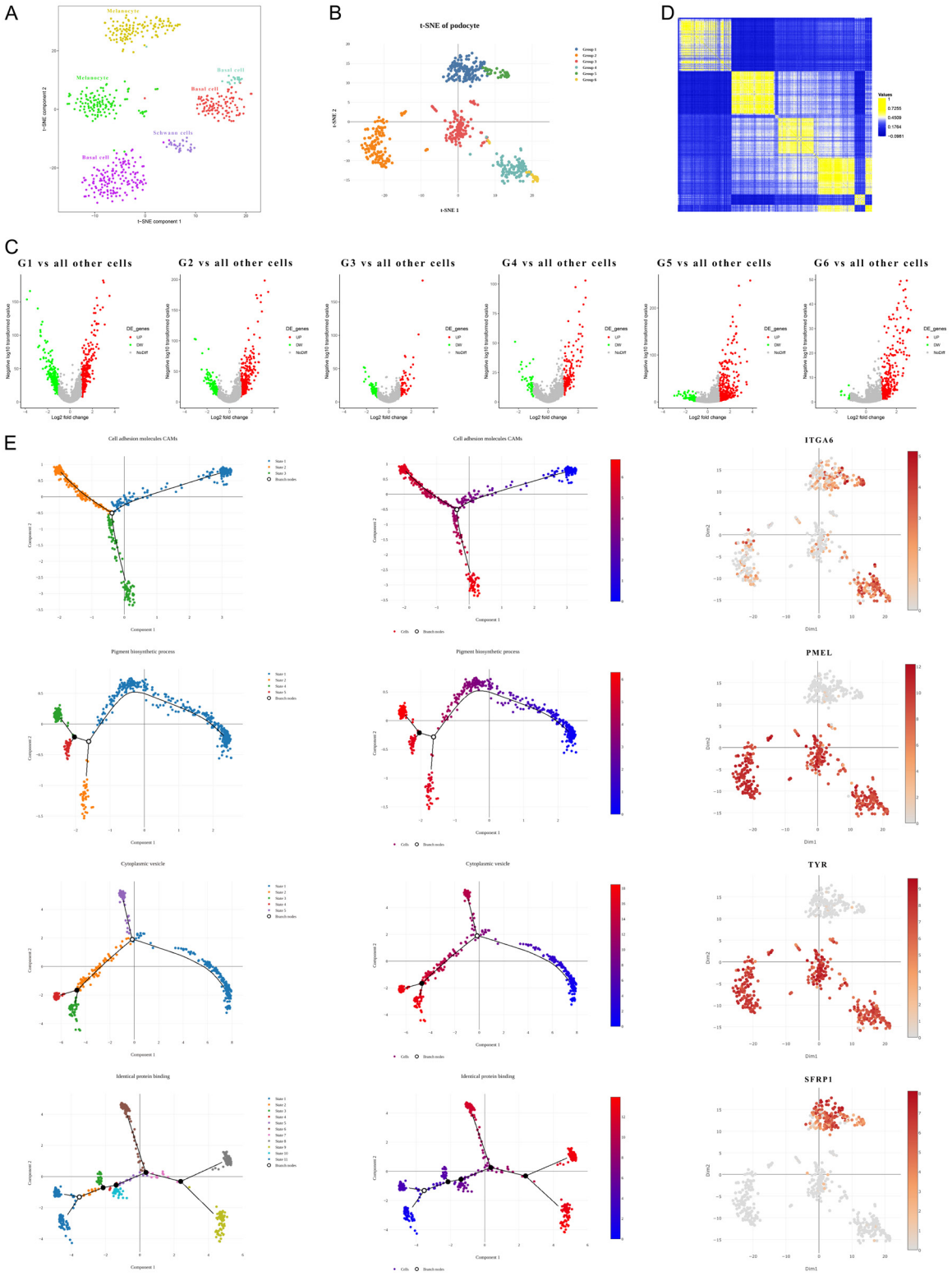

**Figure 10.** The clustering and characteristic description of podocyte subtypes. A and B. The t-SNE plots of 572 podocytes generated from ALONA and ASAP were colored by subtypes. C. The volcano plots of DEGs in each group when compared with other podocytes, each dot represents a gene. The gray ones represent genes without significant difference while the green and red ones represent decreased and increased genes in each group respectively when compared with other podocytes. D. The heatmap of DEGs, the legend for relative expression from lowest expression (blue) to highest expression (yellow) (top right). E. The first two columns are trajectory analysis of melanocytes based on cell adhesion molecules CAMs (pathway), pigment biosynthetic process (BP), cytoplasmic vesicle (CC) and identical protein binding (MF). The last column showed expression of 4 specific genes (ITGA3, ANXA1, CD9 and SERPINA1) via t-SNE. The legends represent different states and levels locate at right. t-distributed stochastic neighbor embedding (t-SNE), differently expressed genes (DEGs), The Cancer Genome Atlas (TCGA).

increased malignancy, the immune defense was disintegrated and tumor microenvironment was no longer suitable for DC survival. Mature DCs are mainly distributed at the pretumorally stage of melanoma further confirming our hypothesis [69].

Although the tumor microenvironment plays an important role in the migration and invasion of melanoma, the essential reason is the presence of malignant cells. In Tirosh et al. research, 1257 malignant cells from 15 tumor samples were screened. In CancerSEA, we found that the gene expression level, copy number of each chromosome and 14 function states (eg. angiogenesis, apoptosis) of each tumor sample were different at single-cell resolution (Figure S14). From this view, the heterogeneity of different samples was confirmed again. Furthermore, by contrasting various DEG-sets of 6 melanocyte subtypes clustered by ALONA, only dopachrome tautomerase (DCT) and apolipoprotein C2 (APOC2) appeared in all DEG-sets. The role of DCT in melanoma has been verified while no evidence could confirm APOC2's function in melanoma [70]. Through analysis in CancerSEA, the correlation between APOC2 and metastasis is significant (correlation strength > 0.3, $P < 0.01$) (Figures S15 and S16). APOC2 participates in the cholesterol metabolism pathway and a low level of cholesterol might inhibit melanoma migration [71]. In one word, APOC2 may play a crucial role in melanocyte heterogeneity.

The microenvironment in melanoma is very complex. The differences between various subtypes in one single cell lineage and the interaction networks between different cell lineages will lead to the specificity of tumor. In the present study, we just provided a brief macroscopic description of the melanoma heterogeneity, so lots of important molecules and networks cannot be described fully. Further research needs to be carried out on melanoma and hopes to provide a new vision for proper therapeutic strategy.

## Acknowledgements

Natural Science Foundation of Sichuan Province (2023NSFSC1552), Natural Science Foundation of China (No. 82002909) and Sichuan Science and Technology Program (2022NSFSC1318).

This study was approved by the the Ludwig Center at Harvard Medical School. All the authors were consent for publication.

## Disclosure of conflict of interest

None.

**Address correspondence to:** Long Chen, Department of Immunology, School of Basic Medical Sciences, Chengdu Medical College, Chengdu 610500, Sichuan, China. E-mail: chenlong@cmc.edu.cn

## References

[1] Hanahan D and Weinberg RA. Hallmarks of cancer: the next generation. Cell 2011; 144: 646-74.

[2] Chan TA, Wolchok JD and Snyder A. Genetic basis for clinical response to CTLA-4 blockade in melanoma. N Engl J Med 2015; 373: 1984.

[3] Aparicio S and Caldas C. The implications of clonal genome evolution for cancer medicine. N Engl J Med 2013; 368: 842-51.

[4] Meacham CE and Morrison SJ. Tumour heterogeneity and cancer cell plasticity. Nature 2013; 501: 328-37.

[5] Shalek AK, Satija R, Adiconis X, Gertner RS, Gaublomme JT, Raychowdhury R, Schwartz S, Yosef N, Malboeuf C, Lu D, Trombetta JJ, Gennert D, Gnirke A, Goren A, Hacohen N, Levin JZ, Park H and Regev A. Single-cell transcriptomics reveals bimodality in expression and splicing in immune cells. Nature 2013; 498: 236-40.

[6] Patel AP, Tirosh I, Trombetta JJ, Shalek AK, Gillespie SM, Wakimoto H, Cahill DP, Nahed BV, Curry WT, Martuza RL, Louis DN, Rozenblatt-Rosen O, Suvà ML, Regev A and Bernstein BE. Single-cell RNA-seq highlights intratumoral heterogeneity in primary glioblastoma. Science 2014; 344: 1396-401.

[7] Macosko EZ, Basu A, Satija R, Nemesh J, Shekhar K, Goldman M, Tirosh I, Bialas AR, Kamitaki N, Martersteck EM, Trombetta JJ, Weitz DA, Sanes JR, Shalek AK, Regev A and McCarroll SA. Highly parallel genome-wide expression profiling of individual cells using nanoliter droplets. Cell 2015; 161: 1202-1214.

[8] Grün D, Lyubimova A, Kester L, Wiebrands K, Basak O, Sasaki N, Clevers H and van Oudenaarden A. Single-cell messenger RNA sequencing reveals rare intestinal cell types. Nature 2015; 525: 251-5.

[9] Tirosh I, Izar B, Prakadan SM, Wadsworth MH 2nd, Treacy D, Trombetta JJ, Rotem A, Rodman C, Lian C, Murphy G, Fallahi-Sichani M, Dutton-Regester K, Lin JR, Cohen O, Shah P, Lu D, Genshaft AS, Hughes TK, Ziegler CG, Kazer SW, Gaillard A, Kolb KE, Villani AC, Johannessen CM, Andreev AY, Van Allen EM, Bertagnolli M, Sorger PK, Sullivan RJ, Flaherty KT, Frederick DT, Jané-Valbuena J, Yoon CH, Rozenblatt-Rosen O, Shalek AK, Regev A and Garraway LA. Dissecting the multicellular ecosystem of metastatic melanoma by single-cell RNA-seq. Science 2016; 352: 189-96.

[10] Picelli S, Björklund ÅK, Faridani OR, Sagasser S, Winberg G and Sandberg R. Smart-seq2 for sensitive full-length transcriptome profiling in single cells. Nat Methods 2013; 10: 1096-8.

[11] Trombetta JJ, Gennert D, Lu D, Satija R, Shalek AK and Regev A. Preparation of single-cell RNA-seq libraries for next generation sequencing. Curr Protoc Mol Biol 2014; 107: 4.22.1-4.22.17.

[12] Li H and Durbin R. Fast and accurate short read alignment with Burrows-Wheeler transform. Bioinformatics 2009; 25: 1754-60.

[13] McKenna A, Hanna M, Banks E, Sivachenko A, Cibulskis K, Kernytsky A, Garimella K, Altshuler D, Gabriel S, Daly M and DePristo MA. The genome analysis toolkit: a MapReduce framework for analyzing next-generation DNA sequencing data. Genome Res 2010; 20: 1297-303.

[14] Berger MF, Lawrence MS, Demichelis F, Drier Y, Cibulskis K, Sivachenko AY, Sboner A, Esgueva R, Pflueger D, Sougnez C, Onofrio R, Carter SL, Park K, Habegger L, Ambrogio L, Fennell T, Parkin M, Saksena G, Voet D, Ramos AH, Pugh TJ, Wilkinson J, Fisher S, Winckler W, Mahan S, Ardlie K, Baldwin J, Simons JW, Kitabayashi N, MacDonald TY, Kantoff PW, Chin L, Gabriel SB, Gerstein MB, Golub TR, Meyerson M, Tewari A, Lander ES, Getz G, Rubin MA and Garraway LA. The genomic complexity of primary human prostate cancer. Nature 2011; 470: 214-20.

[15] Cibulskis K, Lawrence MS, Carter SL, Sivachenko A, Jaffe D, Sougnez C, Gabriel S, Meyerson M, Lander ES and Getz G. Sensitive detection of somatic point mutations in impure and heterogeneous cancer samples. Nat Biotechnol 2013; 31: 213-9.

[16] Ramos AH, Lichtenstein L, Gupta M, Lawrence MS, Pugh TJ, Saksena G, Meyerson M and Getz G. Oncotator: cancer variant annotation tool. Hum Mutat 2015; 36: E2423-9.

[17] Langmead B, Trapnell C, Pop M and Salzberg SL. Ultrafast and memory-efficient alignment of short DNA sequences to the human genome. Genome Biol 2009; 10: R25.

[18] Gardeux V, David FPA, Shajkofci A, Schwalie PC and Deplancke B. ASAP: a web-based platform for the analysis and interactive visualization of single-cell RNA-seq data. Bioinformatics 2017; 33: 3123-3125.

[19] Zhou G, Soufan O, Ewald J, Hancock REW, Basu N and Xia J. NetworkAnalyst 3.0: a visual analytics platform for comprehensive gene expression profiling and meta-analysis. Nucleic Acids Res 2019; 47: W234-W241.

[20] Tang Z, Li C, Kang B, Gao G, Li C and Zhang Z. GEPIA: a web server for cancer and normal gene expression profiling and interactive analyses. Nucleic Acids Res 2017; 45: W98-W102.

[21] Wang Z, Tang W, Yuan J, Qiang B, Han W and Peng X. Integrated analysis of RNA-binding proteins in glioma. Cancers (Basel) 2020; 12: 892.

[22] Shurin MR, Shurin GV, Lokshin A, Yurkovetsky ZR, Gutkin DW, Chatta G, Zhong H, Han B and Ferris RL. Intratumoral cytokines/chemokines/growth factors and tumor infiltrating dendritic cells: friends or enemies? Cancer Metastasis Rev 2006; 25: 333-56.

[23] Jobe NP, Rösel D, Dvořánková B, Kodet O, Lacina L, Mateu R, Smetana K and Brábek J. Simultaneous blocking of IL-6 and IL-8 is sufficient to fully inhibit CAF-induced human melanoma cell invasiveness. Histochem Cell Biol 2016; 146: 205-17.

[24] Michiels C. Endothelial cell functions. J Cell Physiol 2003; 196: 430-43.

[25] Uldry E, Faes S, Demartines N and Dormond O. Fine-tuning tumor endothelial cells to selectively kill cancer. Int J Mol Sci 2017; 18: 1401.

[26] Pisacane AM, Picciotto F and Risio M. CD31 and CD34 expression as immunohistochemical markers of endothelial transdifferentiation in human cutaneous melanoma. Cell Oncol 2007; 29: 59-66.

[27] Schaaf MB, Houbaert D, Meçe O, To SK, Ganne M, Maes H and Agostinis P. Lysosomal pathways and autophagy distinctively control endothelial cell behavior to affect tumor vasculature. Front Oncol 2019; 9: 171.
[28] Thijssen VL, Paulis YW, Nowak-Sliwinska P, Deumelandt KL, Hosaka K, Soetekouw PM, Cimpean AM, Raica M, Pauwels P, van den Oord JJ, Tjan-Heijnen VC, Hendrix MJ, Heldin CH, Cao Y and Griffioen AW. Targeting PDGF-mediated recruitment of pericytes blocks vascular mimicry and tumor growth. J Pathol 2018; 246: 447-458.
[29] Kalluri R. The biology and function of fibroblasts in cancer. Nat Rev Cancer 2016; 16: 582-98.
[30] Özdemir BC, Pentcheva-Hoang T, Carstens JL, Zheng X, Wu CC, Simpson TR, Laklai H, Sugimoto H, Kahlert C, Novitskiy SV, De Jesus-Acosta A, Sharma P, Heidari P, Mahmood U, Chin L, Moses HL, Weaver VM, Maitra A, Allison JP, LeBleu VS and Kalluri R. Depletion of carcinoma-associated fibroblasts and fibrosis induces immunosuppression and accelerates pancreas cancer with reduced survival. Cancer Cell 2015; 28: 831-833.
[31] Sugimoto H, Mundel TM, Kieran MW and Kalluri R. Identification of fibroblast heterogeneity in the tumor microenvironment. Cancer Biol Ther 2006; 5: 1640-6.
[32] Epstein Shochet G, Brook E, Israeli-Shani L, Edelstein E and Shitrit D. Fibroblast paracrine TNF-alpha signaling elevates integrin A5 expression in idiopathic pulmonary fibrosis (IPF). Respir Res 2017; 18: 122.
[33] Xu Y, Xia Q, Rao Q, Shi S, Shi Q, Ma H, Lu Z, Chen H and Zhou X. DCN deficiency promotes renal cell carcinoma growth and metastasis through downregulation of P21 and E-cadherin. Tumour Biol 2016; 37: 5171-83.
[34] Catteau X, Simon P and Noël JC. Stromal expression of matrix metalloproteinase 2 in cancer-associated fibroblasts is strongly related to human epidermal growth factor receptor 2 status in invasive breast carcinoma. Mol Clin Oncol 2016; 4: 375-378.
[35] Truong DD, Kratz A, Park JG, Barrientos ES, Saini H, Nguyen T, Pockaj B, Mouneimne G, LaBaer J and Nikkhah M. A human organotypic microfluidic tumor model permits investigation of the interplay between patient-derived fibroblasts and breast cancer cells. Cancer Res 2019; 79: 3139-3151.
[36] Olumi AF, Grossfeld GD, Hayward SW, Carroll PR, Tlsty TD and Cunha GR. Carcinoma-associated fibroblasts direct tumor progression of initiated human prostatic epithelium. Cancer Res 1999; 59: 5002-11.
[37] Dimanche-Boitrel MT, Vakaet L Jr, Pujuguet P, Chauffert B, Martin MS, Hammann A, Van Roy F, Mareel M and Martin F. In vivo and in vitro invasiveness of a rat colon-cancer cell line maintaining E-cadherin expression: an enhancing role of tumor-associated myofibroblasts. Int J Cancer 1994; 56: 512-21.
[38] Elkabets M, Gifford AM, Scheel C, Nilsson B, Reinhardt F, Bray MA, Carpenter AE, Jirström K, Magnusson K, Ebert BL, Pontén F, Weinberg RA and McAllister SS. Human tumors instigate granulin-expressing hematopoietic cells that promote malignancy by activating stromal fibroblasts in mice. J Clin Invest 2011; 121: 784-99.
[39] Raffaghello L and Dazzi F. Classification and biology of tumour associated stromal cells. Immunol Lett 2015; 168: 175-82.
[40] Murray PJ and Wynn TA. Obstacles and opportunities for understanding macrophage polarization. J Leukoc Biol 2011; 89: 557-63.
[41] Liu Y, Ye Z, Li X, Anderson JL, Khan M, DaSilva D, Baron M, Wilson D, Bocoun V, Ivacic LC, Schrodi SJ and Smith JA. Genetic and functional associations with decreased anti-inflammatory tumor necrosis factor alpha induced protein 3 in macrophages from subjects with axial spondyloarthritis. Front Immunol 2017; 8: 860.
[42] Zhou J, Zheng S, Liu T, Liu Q, Chen Y, Tan D, Ma R and Lu X. IL-1beta from M2 macrophages promotes migration and invasion of ESCC cells enhancing epithelial-mesenchymal transition and activating NF-kappaB signaling pathway. J Cell Biochem 2018; 119: 7040-7052.
[43] Luz-Crawford P, Djouad F, Toupet K, Bony C, Franquesa M, Hoogduijn MJ, Jorgensen C and Noël D. Mesenchymal stem cell-derived interleukin 1 receptor antagonist promotes macrophage polarization and inhibits B cell differentiation. Stem Cells 2016; 34: 483-92.
[44] Liu RH, Wen Y, Sun HY, Liu CY, Zhang YF, Yang Y, Huang QL, Tang JJ, Huang CC and Tang LJ. Abdominal paracentesis drainage ameliorates severe acute pancreatitis in rats by regulating the polarization of peritoneal macrophages. World J Gastroenterol 2018; 24: 5131-5143.
[45] Hussein MR, Elsers DA, Fadel SA and Omar AE. Immunohistological characterisation of tumour infiltrating lymphocytes in melanocytic skin lesions. J Clin Pathol 2006; 59: 316-24.
[46] Muenst S, Läubli H, Soysal SD, Zippelius A, Tzankov A and Hoeller S. The immune system and cancer evasion strategies: therapeutic concepts. J Intern Med 2016; 279: 541-62.
[47] Ladanyi A. Prognostic and predictive significance of immune cells infiltrating cutaneous melanoma. Pigment Cell Melanoma Res 2015; 28: 490-500.
[48] Ladányi A, Kiss J, Mohos A, Somlai B, Liszkay G, Gilde K, Fejös Z, Gaudi I, Dobos J and Tímár J. Prognostic impact of B-cell density in cutane-

ous melanoma. Cancer Immunol Immunother 2011; 60: 1729-38.
[49] Cancer Genome Atlas Network. Genomic classification of cutaneous melanoma. Cell 2015; 161: 1681-96.
[50] Gilbert AE, Karagiannis P, Dodev T, Koers A, Lacy K, Josephs DH, Takhar P, Geh JL, Healy C, Harries M, Acland KM, Rudman SM, Beavil RL, Blower PJ, Beavil AJ, Gould HJ, Spicer J, Nestle FO and Karagiannis SN. Monitoring the systemic human memory B cell compartment of melanoma patients for anti-tumor IgG antibodies. PLoS One 2011; 6: e19330.
[51] Fridman WH, Pagès F, Sautès-Fridman C and Galon J. The immune contexture in human tumours: impact on clinical outcome. Nat Rev Cancer 2012; 12: 298-306.
[52] Gooden MJ, de Bock GH, Leffers N, Daemen T and Nijman HW. The prognostic influence of tumour-infiltrating lymphocytes in cancer: a systematic review with meta-analysis. Br J Cancer 2011; 105: 93-103.
[53] Saizawa K, Rojo J and Janeway CA Jr. Evidence for a physical association of CD4 and the CD3:alpha:beta T-cell receptor. Nature 1987; 328: 260-3.
[54] Chauvin JM, Pagliano O, Fourcade J, Sun Z, Wang H, Sander C, Kirkwood JM, Chen TH, Maurer M, Korman AJ and Zarour HM. TIGIT and PD-1 impair tumor antigen-specific CD8(+) T cells in melanoma patients. J Clin Invest 2015; 125: 2046-58.
[55] Cope AP, Schulze-Koops H and Aringer M. The central role of T cells in rheumatoid arthritis. Clin Exp Rheumatol 2007; 25 Suppl 46: S4-11.
[56] Rosenberg SA, Yang JC and Restifo NP. Cancer immunotherapy: moving beyond current vaccines. Nat Med 2004; 10: 909-15.
[57] Arpaia N, Cassano N and Vena GA. Regressing cutaneous malignant melanoma and vitiligo-like depigmentation. Int J Dermatol 2006; 45: 952-6.
[58] Lanzavecchia A and Sallusto F. Understanding the generation and function of memory T cell subsets. Curr Opin Immunol 2005; 17: 326-32.
[59] Rocha B and Tanchot C. The tower of babel of CD8+ T-cell memory: known facts, deserted roads, muddy waters, and possible dead ends. Immunol Rev 2006; 211: 182-96.
[60] Prlic M, Williams MA and Bevan MJ. Requirements for CD8 T-cell priming, memory generation and maintenance. Curr Opin Immunol 2007; 19: 315-9.
[61] Côté AL, Usherwood EJ and Turk MJ. Tumor-specific T-cell memory: clearing the regulatory T-cell hurdle. Cancer Res 2008; 68: 1614-7.
[62] Coit DG, Thompson JA, Algazi A, Andtbacka R, Bichakjian CK, Carson WE 3rd, Daniels GA, DiMaio D, Ernstoff M, Fields RC, Fleming MD, Gonzalez R, Guild V, Halpern AC, Hodi FS Jr, Joseph RW, Lange JR, Martini MC, Materin MA, Olszanski AJ, Ross MI, Salama AK, Skitzki J, Sosman J, Swetter SM, Tanabe KK, Torres-Roca JF, Trisal V, Urist MM, McMillian N and Engh A. Melanoma, version 2.2016, NCCN clinical practice guidelines in oncology. J Natl Compr Canc Netw 2016; 14: 450-73.
[63] Vizkeleti L, Kiss T, Koroknai V, Ecsedi S, Papp O, Szasz I, Adany R and Balazs M. Altered integrin expression patterns shown by microarray in human cutaneous melanoma. Melanoma Res 2017; 27: 180-188.
[64] Boudhraa Z, Merle C, Mazzocut D, Chezal JM, Chambon C, Miot-Noirault E, Theisen M, Bouchon B and Degoul F. Characterization of pro-invasive mechanisms and N-terminal cleavage of ANXA1 in melanoma. Arch Dermatol Res 2014; 306: 903-14.
[65] Fan J, Zhu GZ and Niles RM. Expression and function of CD9 in melanoma cells. Mol Carcinog 2010; 49: 85-93.
[66] Kwon CH, Park HJ, Choi JH, Lee JR, Kim HK, Jo HJ, Kim HS, Oh N, Song GA and Park DY. Snail and serpinA1 promote tumor progression and predict prognosis in colorectal cancer. Oncotarget 2015; 6: 20312-26.
[67] Nagata M. Podocyte injury and its consequences. Kidney Int 2016; 89: 1221-30.
[68] Nedelcu RI, Ion DA, Holeab CA, Cioplea MD, Brînzea A and Zurac SA. Dendritic cells in melanoma - immunohistochemical study and research trends. Rom J Morphol Embryol 2015; 56: 997-1002.
[69] Kobayashi M, Suzuki K, Yashi M, Yuzawa M, Takayashiki N and Morita T. Tumor infiltrating dendritic cells predict treatment response to immmunotherapy in patients with metastatic renal cell carcinoma. Anticancer Res 2007; 27: 1137-41.
[70] Filimon A, Zurac SA, Milac AL, Sima LE, Petrescu SM and Negroiu G. Value of dopachrome tautomerase detection in the assessment of melanocytic tumors. Melanoma Res 2014; 24: 219-36.
[71] Costa GA, de Souza SB, da Silva Teixeira LR, Okorokov LA, Arnholdt ACV, Okorokova-Façanha AL and Façanha AR. Tumor cell cholesterol depletion and V-ATPase inhibition as an inhibitory mechanism to prevent cell migration and invasiveness in melanoma. Biochim Biophys Acta Gen Subj 2018; 1862: 684-691.
[72] Badylak SF, Valentin JE, Ravindra AK, McCabe GP and Stewart-Akers AM. Macrophage phenotype as a determinant of biologic scaffold remodeling. Tissue Eng Part A 2008; 14: 1835-42.

[73] Spiller KL, Anfang RR, Spiller KJ, Ng J, Nakazawa KR, Daulton JW and Vunjak-Novakovic G. The role of macrophage phenotype in vascularization of tissue engineering scaffolds. Biomaterials 2014; 35: 4477-88.
[74] Hao NB, Lü MH, Fan YH, Cao YL, Zhang ZR and Yang SM. Macrophages in tumor microenvironments and the progression of tumors. Clin Dev Immunol 2012; 2012: 948098.
[75] Wilson HM. SOCS proteins in macrophage polarization and function. Front Immunol 2014; 5: 357.
[76] Gordon S and Taylor PR. Monocyte and macrophage heterogeneity. Nat Rev Immunol 2005; 5: 953-64.
[77] Stöger JL, Gijbels MJ, van der Velden S, Manca M, van der Loos CM, Biessen EA, Daemen MJ, Lutgens E and de Winther MP. Distribution of macrophage polarization markers in human atherosclerosis. Atherosclerosis 2012; 225: 461-8.
[78] Yamaguchi H, Lorenz M, Kempiak S, Sarmiento C, Coniglio S, Symons M, Segall J, Eddy R, Miki H, Takenawa T and Condeelis J. Molecular mechanisms of invadopodium formation: the role of the N-WASP-Arp2/3 complex pathway and cofilin. J Cell Biol 2005; 168: 441-52.
[79] Chávez-Galán L, Olleros ML, Vesin D and Garcia I. Much more than M1 and M2 macrophages, there are also CD169(+) and TCR(+) macrophages. Front Immunol 2015; 6: 263.
[80] Roszer T. Understanding the mysterious M2 macrophage through activation markers and effector mechanisms. Mediators Inflamm 2015; 2015: 816460.